

Flow-induced alignment of lamellar block copolymer melts

Zhong-Ren Chen and Julia A. Kornfield*

Chemical Engineering 210-41, California Institute of Technology, Pasadena, CA 91125, USA

(Received 18 December 1997; revised 14 January 1998; accepted 14 January 1998)

Toward the integrated synthesis and processing of functional block copolymer nanostructures, the physics of flow-induced alignment of block copolymers must be understood to predict the direction, rate and degree of alignment. In this review we focus on key issues regarding flow-induced alignment of lamellae. A three-dimensional mapping summarizes previous results on the selection of alignment directions (parallel or perpendicular) and their pathways in terms of three dimensionless parameters: frequency, temperature and strain amplitude. Trajectories, kinetics and structural evolution are explored in a fourth dimension (time). The challenge of developing adequate experimental methods for monitoring transient structure is discussed. A comprehensive experimental approach, which combines *in-situ* rheo-optical measurements and *ex-situ* structural characterization by electron microscopy and X-ray scattering, is presented as a new tool for tracking changes of microstructure and orientation during flow-induced alignment. Various mechanisms that have been proposed over the past two decades are reviewed and re-evaluated based on recent experimental results. Outstanding questions and new issues raised by ABC triblock copolymer nanostructures are discussed. © 1998 Elsevier Science Ltd. All rights reserved.

(Keywords: SAXS; SANS; TEM)

INTRODUCTION

Nanostructural engineering represents a new avenue for improving the performance of materials such as metals¹, polymers^{2–4}, ceramics⁵ and those beyond traditional classification^{6–8}. Advances in understanding the chemistry and physics of materials provide the tools for synthesis and structural manipulation^{1–10}. Without altering the chemical composition, introduction of the desired microstructure can enhance or even create outstanding properties from a traditional material. Self-assembly, among other approaches, provides a versatile means to create desired nanostructures in bulk materials or at interfaces, with potential applications in biomaterials^{6,10,11}, optics¹² and microelectronics¹³. This review deals with a particular class of self-assembled materials, block copolymers, that offer control of the form and size of their local nanostructure by design of the macromolecular architecture^{3,9,10,14–20}. These polymers are also amenable to producing materials in which the local structure can be aligned over macroscopic dimensions and the number of defects in the local structure can be drastically reduced through processing²¹. The dynamics of macroscopic alignment are critical in tailoring materials' structure and properties and is the focus of the present review.

Block copolymers (BCPs) represent an important class of microstructurally engineered materials in large part because their morphology and dynamics can be systematically controlled by choosing the blocks' compositions and relative lengths^{14–30}. For example, diblock copolymers consisting of two flexible but chemically different segments can form cubic arrays of spheres, hexagonal arrays of

cylinders, bicontinuous cubic phases or lamellae, depending on the relative lengths of the blocks²⁰. Self-assembly of block copolymers can be combined with the orientational ordering tendencies of liquid crystalline polymers (LCP) by synthesizing polymers in which at least one block is an LCP^{27,28,31}. For rod-coil diblock copolymers, interesting zigzag and arrowhead morphologies have been observed²⁷. Greater diversity in the form of the nanostructure can be achieved by connecting three distinct blocks to form ABC triblock copolymers, which assemble such sophisticated structures as helical strands surrounding cylinders in a continuous matrix^{14–16}. Confinement within the self-assembled nanostructure of a block copolymer can be used to affect further structure development within it, such as the subsequent crystallization of one of the blocks²⁹. Similarly, the form of the BCP nanostructure can be used as a template for the synthesis of a solid by polymerization of an epoxy³⁰ or by controlled nucleation and growth of inorganic particles³².

Self-assembly of BCPs typically leads to local order. This local order can be extended to the macroscale by processing using applied fields to achieve directional properties, such as transport, optical and electrical properties. Recently, in a diblock copolymer consisting of polystyrene and a side-chain ferroelectric liquid crystalline polymer, bistable ferroelectric switching was detected in an aligned lamellar material, though there is no ferroelectric response without orientation²⁸. Symmetry-breaking fields, such as flow and electric fields have been used to induce alignment^{2,21–26,33–65}. Flow provides an efficient and versatile means of achieving global alignment, as demonstrated by materials subjected to extrusion²⁴, oscillatory and steady shear^{25,26,39–63}, extensional flow⁶⁴ and roll-casting⁶⁵. Further, the alignment direction of lamellae may switch

* To whom correspondence should be addressed

by 90° with a small change in processing conditions³⁹. This ‘flipping’ phenomenon may ultimately provide responsive, switchable material properties.

The physical basis of the effects of molecular architecture and processing conditions must be understood for the integrated synthesis and processing of functional materials based on aligned block copolymer nanostructures. For example, which type of flow is the most effective in inducing global order? Which parameters control the direction, rate and perfection of alignment for a specific type of block copolymer? How do we design a block copolymer so that directional properties can be achieved by convenient processing conditions? To address these critical issues, investigations are underway to determine the effect of flow conditions and macromolecular characteristics on the direction^{2,39–50,63}, rate^{49,51,63} and mechanisms^{2,25,26,35,39,47,55,63} that lead to macroscale order. Scattering, microscopy and rheo-optical methods are used to characterize the form and orientation distribution of these nanostructures under shear. Unfortunately, any one of these methods alone cannot provide all of the necessary structural information. Scattering does not provide adequate time resolution, microscopic methods such as TEM are not *in-situ* methods and rheo-optical methods are not capable of capturing detailed structural information. A combination of real-time rheo-optical methods with *ex-situ* structural characterization using both SAXS and TEM has provided new insight into the physics of alignment, establishing a framework for understanding much of the alignment behaviour of lamellar BCPs^{2,63}.

This review focuses on recent progress in the physics of flow-induced alignment in lamellar block copolymers. Only oscillatory shear is discussed, since it permits systematic investigation of the coupled effects of the rate and amplitude of deformation in relation to the relaxation dynamics of the self-assembled nanostructure. The extensive body of experimental results on the dynamics of lamellar systems in particular permits a critical evaluation of the concepts that have been put forward to explain their alignment behaviour. Comprehensive reviews are available for general aspects of the thermodynamics²⁰ and dynamics^{21,22} of block copolymer melts and solutions. The present article is divided into five sections: (1) basic concepts regarding the direction and types of lamellar alignment, conditions that induce each type of alignment and their relationship to the intrinsic dynamical properties of BCPs; (2) experimental approaches to test these basic concepts; (3) distinct alignment trajectories, their kinetics and the evolution of structure during the alignment process; (4) mechanisms of flow-induced alignment; and (5) the effects of different polymer architectures on flow behaviour. The fundamental physics of alignment discussed in the first four sections is based mainly on investigations of polystyrene–polyisoprene (PS–PI) diblock copolymers, since this model system is suitable to almost all types of experimental methods, including rheo-optical, X-ray and neutron scattering, and transmission electron microscopy, and has been studied most intensively. Among the effects of polymer architecture, particular attention is given to ABC triblock copolymers, since they are able to form complex and interesting nanostructures. To close, we highlight the implications of current work and offer some suggestions for future studies.

BASIC CONCEPTS OF FLOW-INDUCED ALIGNMENT

Large amplitude oscillatory shear (LAOS) can produce

either ‘parallel’ or ‘perpendicular’ alignment in a nearly symmetric poly(ethylene-propylene)–poly(ethylene) (PEP–PEE) (*Figure 1*) and PEP–PEE-type BCPs (such as PEP–PE)^{39,40,46}. This ‘flipping’ phenomenon is also observed in PS–PI and other PS–PI-type BCPs (styrene–diene BCPs and their hydrogenated counterparts)^{2,39–50,63}. To explain the observed frequency-dependent alignment behaviour, two characteristic frequencies have been proposed: the frequency above which the distortion of chain conformation dominates the materials’ viscoelasticity (ω_c')^{46,47,49,66–69}; and the frequency below which the relaxation of domains becomes significant (ω_d). Between ω_c' and ω_d the distortion of the nanostructure dominates the viscoelastic response of the material.

Four frequency regimes have been found, and different types of alignment dominate in each regime. Perpendicular alignment may be induced by shearing at frequencies that couple with the dynamics of the nanostructure, i.e. frequencies too fast for domain-scale relaxation, but slow enough that chain conformation is relaxed ($\omega_d < \omega < \omega_c'$) (Regime I). Two regimes exist at higher frequencies $\omega > \omega_c'$ that are associated with parallel alignment, but through two qualitatively different pathways. At frequencies slightly above ω_c' , parallel alignment occurs through a transient orientation distribution that consists of parallel and perpendicular orientations and the range of orientations between the two (Regime II: $\omega_c' < \omega < 10 \times \omega_c'$). Frequencies far above ω_c' can also induce parallel alignment, but through bimodal distributions rich in parallel and transverse orientations (Regime III: $\omega > 10 \times \omega_c'$). At low frequencies (Regime IV: $\omega < \omega_d$) the alignment direction tends to be parallel in some systems (e.g. PEP–PEE-type)^{39,40,46} and perpendicular in others^{2,41,42,44,47,49,50,63} (such as PS–PI-type, except following a specific thermal treatment: prolonged annealing close to the BCPs’ upper glass transition^{48,55,56}). Within each regime, strain amplitude affects the rate and degree of alignment, and the direction of alignment; strain amplitude can even alter the direction of alignment, particularly if the frequency is in the vicinity of the boundary between Regimes I and II⁵⁰ and perhaps near the boundary between Regimes IV and I⁵⁸. The complex interplay of temperature, frequency and strain amplitude can be represented using a three-dimensional mapping (*Figure 1*). Rich information on the way alignment occurs is manifested in the additional dimension of time. Within a given frequency regime (Regime I, II or III),* the time evolution of microstructures follows a particular type of trajectory^{49,50}. For each trajectory, the initial fast process is responsible for the selective creation of layers, while the later slow process is responsible for selective elimination of all orientations but one, and leads to the final unidirectional, single-crystal-like structure⁶³.

Theoretical explanations of the alignment regimes focus on the relative stability of distinct well-aligned states. The transverse alignment is most unstable, since the equilibrium spacing is disturbed by shearing. Fluctuations on a layered structure can couple to shear if the lamellae are in the parallel orientation, making this alignment less stable than perpendicular^{33,34}. However, the effect of fluctuations will

* There is one family of trajectories in Regime IV that remains to be investigated in the future: the route to parallel alignment at very low frequencies, $\omega < \omega_d$. This regime has been studied by rheo-optical techniques in PEP–PEE-2, but this system is not amenable to transmission electron microscopy. In PS–PI, this regime is not accessible without a prolonged annealing treatment.⁵⁶

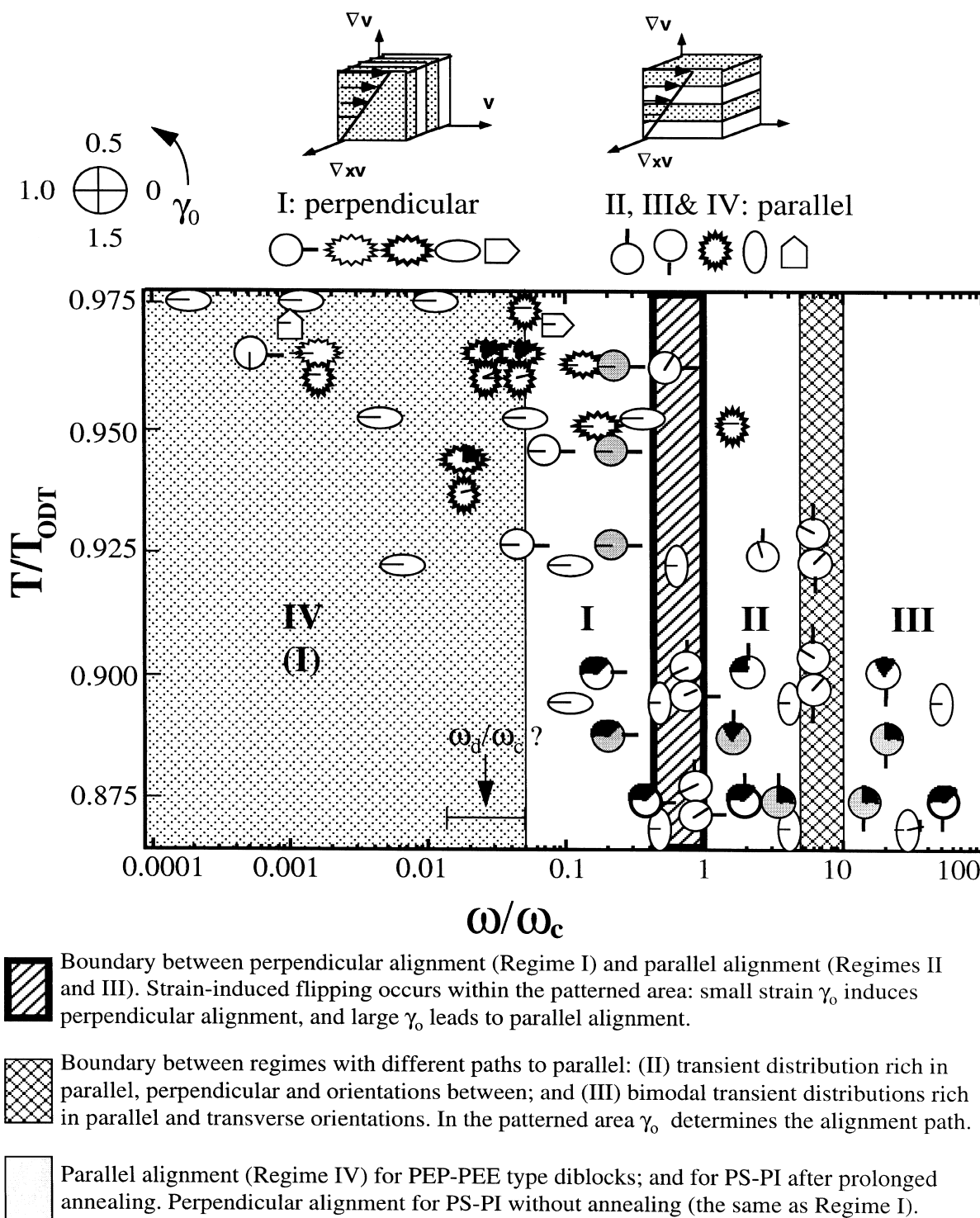


Figure 1 Three-dimensional mapping of LAOS flow-induced alignment regimes in terms of temperature, frequency and strain amplitude. The third dimension (strain amplitude) is shown inside the symbols using the scale indicated in the upper right corner: the strain amplitude used is indicated by the orientation of the mark within the symbol; a solid wedge indicates the range and strain amplitudes. Results on PS-PI are shown as circles^{49,50,63,72}, ellipses^{41,47} and modulated ellipses^{48,56,58} (those with a thick line represent annealed samples). Rectangular arrowheads represent PEP-PEE results^{39,46}. Dimensionless frequencies are computed using ω_c' based on the storage modulus method (Figure 2a) wherever possible^{41,47,49,50,63,72}. The range of ω_d/ω_c' indicated is based on values given by Koppi *et al.*³⁹ and Wiesner *et al.*^{48,55,56}

be confined to frequencies fast enough that the fluctuations are not averaged out ($\omega > \omega_d$) and slow enough that distortion of the nanostructure is not overwhelmed by more local responses, such as conformational distortion of the polymer chains ($\omega < \omega_c'$). These concepts are in accord with the observation that perpendicular alignment is induced by deformation frequencies at which the dynamics are dominated by the layered nanostructure ($\omega_d < \omega < \omega_c'$,

'lamellar regime') (Figure 2) and at temperatures in proximity to the the order-disorder transition temperature (ODT)³⁹. Parallel alignment is predicted to be more stable than perpendicular below a critical frequency controlled by the characteristic lifetime of fluctuations ($\omega < \omega_d$)³³. These arguments can describe the experimentally observed behaviour of the PEP-PEE system³⁹.

In order to explain parallel alignment at higher frequencies

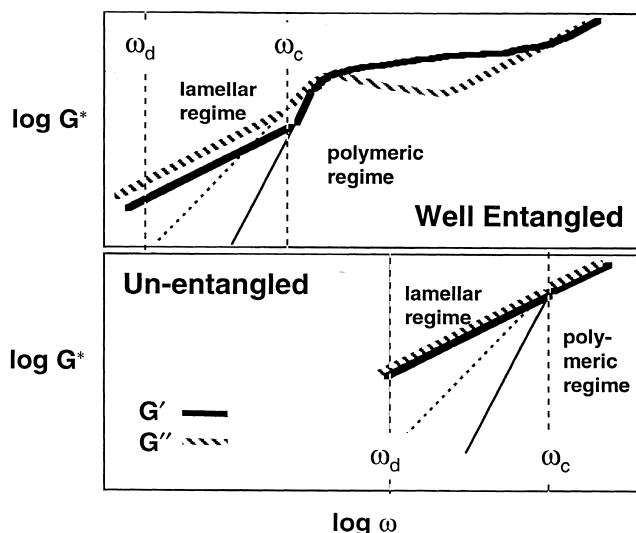


Figure 2 Dynamic regimes of block copolymers: distortion of chain conformation dominates the viscoelastic properties in the 'polymeric regime' ($\omega > \omega_c$); distortion of the ordered structure, here lamellae, dominates in the 'lamellar regime' ($\omega_d < \omega < \omega_c$). At much lower frequency there must exist a slow enough frequency that defects can move and domains can respond (ω_d). The value of ω_d and the dynamics that dominate at $\omega < \omega_d$ are poorly understood. In the polymeric regime, the heavy lines represent the dynamic moduli of both the disordered and ordered, but unaligned, states. In the lamellar regime the ordered, but unaligned, state has higher storage and loss moduli (bold lines) than the disordered state (narrow lines). Diblocks with very small X_{AB} can be made long enough to be well entangled (top) while still having accessible ODT (e.g. PEP-PEE-type polymers). When X_{AB} is larger, the length of the diblock must be kept short to have an accessible ODT; such diblocks are usually not entangled (bottom) (e.g. PS-PI-type polymers). These dynamic regions appear to correspond to distinct alignment regimes (see text)

($\omega > \omega_c'$) for PS-PI and other similar systems, the concept of viscoelastic contrast has been introduced⁴⁷. At frequencies faster than the conformational relaxation of the chains ($\omega > \omega_c'$), the deformation couples to more local dynamics, and differences between the types of layers in the ordered structure can be probed. If there is considerable difference in the mechanical properties of the two types of layers (such as with PS-PI), the modulus of the parallel state is lower than that of the perpendicular state, and this may explain the selection of parallel alignment. Thus, three frequency regimes have been identified: $\omega < \omega_d$ where parallel alignment can be induced, $\omega_d < \omega < \omega_c'$ where perpendicular alignment can be induced, and $\omega_c' < \omega$ where parallel alignment can be induced in lamellar arrays in which the layers have dissimilar viscoelastic properties.

These concepts regarding the relative stability of monodomains have provided a valuable guide to experiment. They explain three frequency regimes based on the final alignment direction. But concepts that deal with differently oriented monodomains are not sufficient to clarify the mechanisms of alignment. This is illustrated by the existence of at least two qualitatively different routes to the same final state, e.g. parallel at $\omega > \omega_c'$.

To understand pathways to alignment, concepts regarding the mechanisms of orientation selection and defect dynamics have been put forward since the early 1970s. In the early work of Keller and Hadziioannou, the concepts of grain rotation, anisotropic viscoelasticity, selective melting and defect migration have been considered^{24,25}. The selective melting hypothesis has taken on a special role in explaining the development of perpendicular alignment under conditions close to the ODT³⁹. It has also been

suggested that two or more mechanisms may act in combination to produce alignment^{25,26,41}. However, *in-situ* information was not available to examine the validity and relative importance of these ideas. Further, these concepts need to be made more specific in order to assist theoretical advances. For example, what type of defects dominate? Does the answer depend on flow conditions (ω , T)? Does the relative importance of different types of defects change as the system moves through the alignment process?

To answer these questions, developing appropriate experimental methods to characterize the transient structure is crucial. In addition, methods of determining the characteristic frequencies ω_c' and ω_d are needed to test theories regarding the frequency regimes that lead to particular alignment. Therefore, before we review recent progress in understanding the nature and kinetics of alignment processes, we first discuss the experimental tools that exist and their current limitations.

EXPERIMENTAL NEEDS AND APPROACHES

Our discussion of the experimental approaches used to test the basic concepts of flow-induced alignment begins with methods of determining ω_c' and ω_d using melt rheology and optical rheometry. As has been pointed out, ω_c' appears to define one of the key boundaries, between Regimes I and II; ω_d may be related to the relaxation of domains and may define the boundary between Regimes IV and I. The evolution of structure during shearing provides direct information on the mechanisms of alignment, so experimental approaches to characterizing the time evolution of structures under shear will be addressed. We close this section by commenting briefly on the characterization of well-aligned states.

Determination of characteristic frequencies

Developing robust, reproducible and precise experimental methods to determine ω_c' and ω_d is of practical importance in locating alignment behaviour in the frequency spectrum for a given polymer. So far there is only one method for determining the parameter ω_c' that meets these criteria. The storage modulus ($G'(\omega)$) of the ordered, but unaligned state is compared with that of the disordered material, and ω_c' is determined as the frequency below which the ordered state has a substantially larger modulus than the disordered material (Figure 3a)^{47,66,70}. At these low frequencies the unaligned, ordered material usually has $G'(\omega) \propto \omega^{0.5 \pm 0.1}$ and the disordered material is in its terminal region where $G'(\omega) \propto \omega^2$. The uncertainty in determining ω_c' is small, since it can be determined by the intercept of lines with very different slopes in a log-log plot of G' versus ω ^{47,66}. This method can also be applied by comparing ordered but partially aligned states to the disordered state; similar values of ω_c' are obtained⁴⁷, but the uncertainty is somewhat larger, since alignment shifts the dynamic moduli of the ordered material toward those of the disordered phase. The method applies to diblocks of both PEP-PEE^{46,66} and PS-PI^{47,49,51,63} types, ABA triblocks^{44,71}, and even two-nanophase-separated ABC triblocks⁷². There are some limitations related to this method: it requires an accessible ODT for the BCP and is valid only for a limited range of molecular size. As molecular weight increases, extrapolation is needed for some systems (Figure 3b)^{49,63}. Since the order-disorder transition temperature T_{ODT} increases dramatically with the block copolymer length, chain relaxations become so fast in the disordered state that they can move out of the experimentally accessible frequency range.

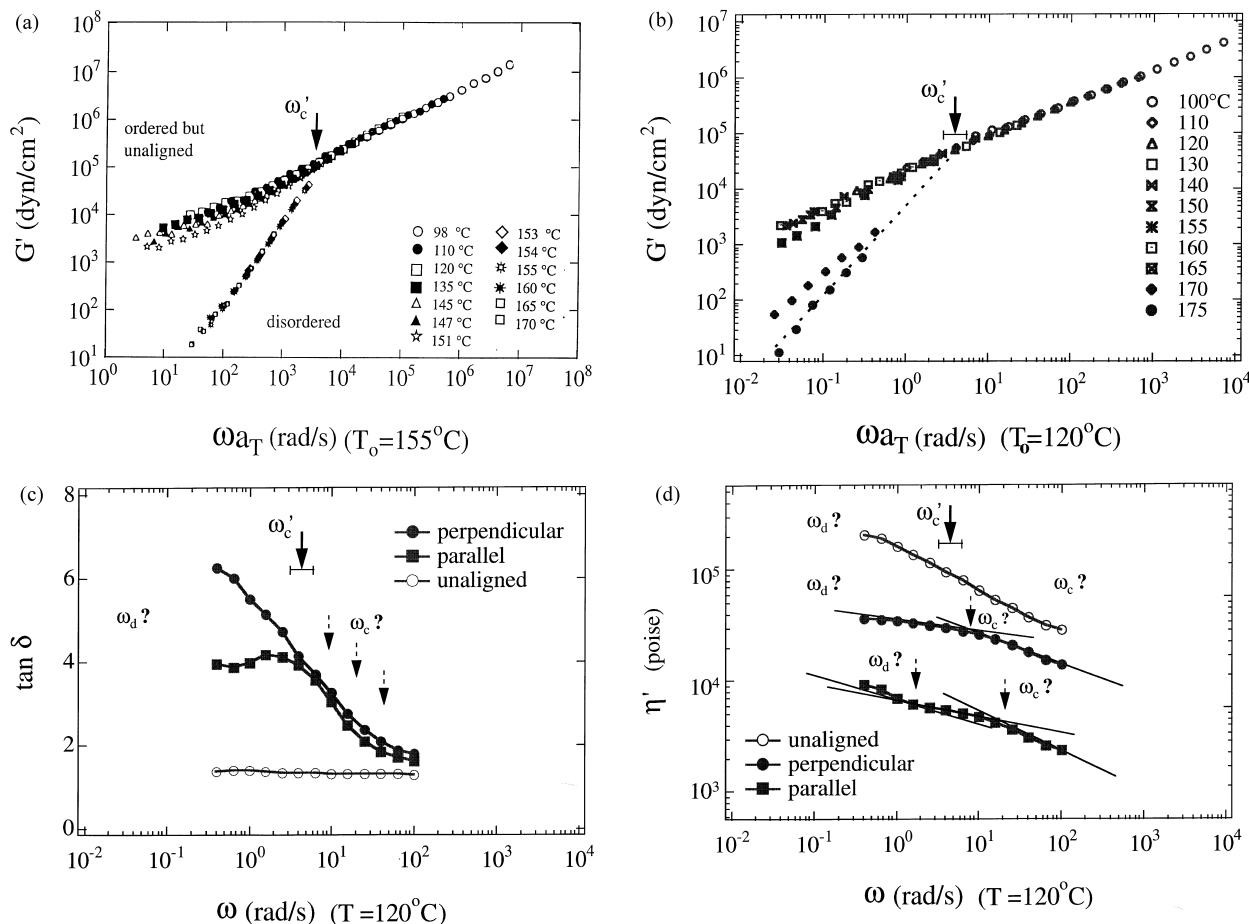


Figure 3 Various methods of determining ω_c' and ω_d from the melt rheology of block copolymers (see text for details). (a) Determination of ω_c' from $G'(\omega)$ is illustrated for a PS-PI (12.5K-9.5K) diblock copolymer⁴⁷. (b) The same method for determining ω_c' requires extrapolation for a PS-PI (10K-10K)⁶³. (c) The loss tangent method for estimating ω_c and ω_d for a PS-PI (10K-10K) diblock copolymer. (d) The dynamic viscosity method for determining ω_c and ω_d for an unaligned PS-PI (10K-10K) diblock copolymer. Parts (c) and (d) use data at a single temperature to eliminate any uncertainty in time-temperature shifting. The value of ω_c' shown is the same as in part (b)

To overcome these limitations, Kannan *et al.*⁴⁶ determined $\omega_{c,so}'$ (very close to ω_c') using a rheo-optical method. For a block copolymer in which the intrinsic contribution dominates the birefringence, the stress-optical rule holds above a particular frequency $\omega_{c,so}'$. Above this frequency distortion of chain conformation dominates both the stress and birefringence. Thus, ω_c' was identified without heating the sample over T_{ODT} . However, this method is valid only for polymers that have much greater intrinsic birefringence than form birefringence, such as PEP-PEE. Further, the measurements should be made in the ordered but unaligned state, since shear-induced alignment shifts $\omega_{c,so}'$ to lower frequencies. Reliable preparation of this ordered but unaligned state requires an accessible ODT.

As to the other important frequency ω_d , Koppi *et al.*³⁹ evaluated it for PEP-PEE, using a perpendicularly aligned sample and an unaligned sample, by measuring the storage modulus in the shear plane (G_{yz}'). A small 'bump' in the frequency dependence of G_{yz}' of the perpendicularly aligned sample was attributed to defect motions. Kannan *et al.* noticed that the value of $\omega_{c,so}''$ was very close to ω_d evaluated by Koppi *et al.*; thus, it may be possible to estimate ω_d by rheo-optical methods as well. Although these approaches provide a rough estimate of ω_d , determination of a meaningful value of ω_d requires that it be measured for a well-defined state. It is believed that ω_d is controlled by grain boundaries and defects^{39,46,68} and is not an intrinsic

property; its value would depend on the domain size^{46,68}, since increasing the domain size could reduce this cut-off frequency⁶⁸. Thus, it is important that the condition for characterizing the domain structure be highly reproducible. This is readily achieved when all previous flow and thermal history has been erased, i.e. using an unaligned sample obtained by ordering in the absence of aligning field. Alternatively, one might consider a final, well-aligned structure as a potential reference state. However, in terms of physical meaning, a measure of domain or defect dynamics only makes sense for polydomain samples. A truly 'well-aligned' material (see next section), while reproducible, would not provide a meaningful value of ω_d .

Progress is needed to overcome the limitations of the existing methods of determining ω_c' and ω_d . Zhang *et al.*^{48,55,56} have suggested alternative methods of estimating ω_c and ω_d using the loss tangent ($\tan \delta = G''/G'$) and dynamic viscosity ($\eta' = G''/\omega$). They estimate ω_c and ω_d as the upper and lower points in the $\tan \delta$ versus $\log \omega$ curve between which $\tan \delta$ has a loss peak (Figure 3c), or as the upper and lower limits in the \log - \log plot of η' versus ω beyond which η' has a stronger dependence on frequency (Figure 3d). These methods seem not to work for polymers that are not entangled, such as a lamellar PS-PI with an accessible ODT. For example, consider the application of these methods to a PS-PI block copolymer that has a molecular weight close to those used in most of the

literature (Figure 3b,c,d)^{2,41–44,47–51,54,56–58,63}. This BCP lacks an entanglement plateau, and it is impossible to locate ω_c using the loss tangent, especially for the ordered but unaligned state, since it is almost a flat line rather than a curve (Figure 3c). Using $\eta'(\omega)$, it is equally difficult to determine ω_c (Figure 3d). For the two aligned states (parallel and perpendicular), the values of ω_c estimated using these suggested methods vary with the alignment direction (Figure 3d, $\omega_{c, \text{parallel}} > \omega_{c, \text{perpendicular}}$). A rough estimate of ω_d is made for a parallel aligned sample, since it shows a hint of a loss peak; however, there is inherently a large uncertainty, since there are no criteria for selecting a particular frequency on the low frequency side of the loss peak (Figure 3c) and the inflection in η' is very slight. The values of ω_c' extracted from these two methods (Figure 3cd) are inconsistent with each other and differ significantly from the value obtained with the well-defined method described above (Figure 3b). As mentioned before, ω_c is an intrinsic parameter and does not depend on the state of samples. Indeed, almost the same value of ω_c' is obtained for unaligned, parallel aligned and perpendicular aligned samples when using the storage modulus method⁴⁷. Thus, the proposed methods of determining ω_c based on the loss tangent and dynamic viscosity are not as precise or robust as the storage modulus method.

Flow-induced alignment trajectories below and above ω_c' are well-defined (boundary between Regimes I and II in Figure 1), since ω_c' can be determined by the storage modulus method; however, it is very difficult to locate regimes based on ω_d (boundary between Regimes I and IV). Parallel alignment has been observed for PEP-PEE type diblocks at $\omega < 0.03 \times \omega_c'$ (presumed to be $\omega < \omega_d$), while perpendicular alignment can still be induced at very low frequency for PS-PI diblocks (as low as $0.0001 \times \omega_c'$)^{47,49,51}. Perhaps this is due to a difference between the values of ω_d/ω_c' for the two systems, since their textures and domain sizes might not be the same. Parallel alignment has been reported in a lamellar PS-PI in the frequency range $0.01 \times \omega_c < \omega < 0.1 \times \omega_c$, if the samples were pressed and annealed prior to shearing⁵⁶. However, parallel alignment can be induced by pressing and annealing even without subsequent shearing^{52,61,64,73}.

In summary, the determination of ω_c' is straightforward for samples with accessible ODT. Further improvements are needed for methods of determining ω_c' when the ODT is not accessible and of determining ω_d in general.

Characterization of the time evolution of microstructure

A variety of experimental methods are used for characterizing the evolution of structure during flow alignment. The advantages and limitations of each method are discussed here in terms of suitability for *in-situ* studies, richness of the information that can be extracted and possible artifacts. Electron microscopy, X-ray and neutron scattering and rheo-optics will be the methods of interest. Finally, we comment on a combined approach that takes advantage of the usefulness of individual methods while minimizing their limitations.

Electron microscopy is uniquely suited to imaging the type and density of defects that define the domain structure in a block copolymer^{26,41,42,45,53,54,63,73–75}. The length scale of interest ranges from tens of nanometers, for the initial condition in an unaligned material obtained by moving through the ODT with no aligning field^{41,63}, up to micron scale as defects are almost completely eliminated from the material^{54,63}. By carefully following the sample orientation

during microsectioning and imaging, the orientations of the lamellae relative to the flow geometry can be obtained as well^{41,42,63}. Three limitations of TEM are: (1) the structure of the material may be altered by sectioning, staining and imaging with high energy electron beams, (2) only a small area in the sample can be viewed at a time, so it is difficult to get a statistical view of the degree of alignment, and (3) it is not attractive for kinetic studies, since electron microscopy is not an *in-situ* method. The first two limitations may be alleviated by using field emission gun scanning electron microscopy (FG-SEM)⁵³. In spite of its limitations, no other techniques could replace electron microscopy, since this is the only method that records the local structure in the material.

X-ray and neutron scattering applied along all three axes of the flow geometry^{2,40,55,63} provide detailed information on the dimensions of the nanostructure and the shape of its orientation distribution. The progression of structure at intermediate states of flow-induced alignment in PS-PI-type systems is captured by cooling through the BPC's upper glass transition temperature, then removing the sample for characterization^{2,26,40–42,44,45,53–55,63,73–75}. While the results provide a sampling of complex microstructural changes induced by shearing, they have some significant limitations. Like TEM, three-axis SAXS/SANS cannot be performed *in situ*, so both methods have poor time resolution and suffer from uncertainties in the relaxation of structure after cessation of shearing, and any distortion of structure during unloading and subsequent sample preparation. Further, in most studies that have used *ex-situ* characterization methods, little information was available to guide the selection of sampling conditions^{26,55}. Typically the rheological signature of alignment was the only *in-situ* measurement; unfortunately, the rheological properties often vary weakly and even non-monotonically with substantial changes in alignment⁴⁹. Thus, it has been difficult to interpret prior results in the context of an overall alignment trajectory, or to view the structural development along a particular path to alignment in the context of distinct families of alignment trajectories.

The challenges associated with *ex-situ* studies have motivated the development of *in-situ* methods that use SAXS^{40,45} SANS,^{61,62} or polarimetry^{2,46,49–51,63} to monitor flow-induced alignment. *In-situ* scattering methods are most frequently applied along a single axis⁷¹; using a Couette geometry, it is possible to monitor scattering in both the $(\nabla \mathbf{v}, \nabla \times \mathbf{v})$ - and $(\mathbf{v}, \nabla \times \mathbf{v})$ -planes^{60,62}. The time resolution of both SAXS and SANS continues to improve, and scattering patterns acquired tens to hundreds of seconds apart have been reported^{62,71}. Flow-induced alignment can occur on a timescale of seconds, which requires *in-situ* probes that have much greater speed. In addition, limited access to synchrotron and neutron beam time motivates *in-situ* measurements that can be made using more readily available instrumentation.

Since there are many factors that affect alignment kinetics, larger numbers of experiments are needed to map transient behaviour as a function of multiple parameters. Therefore, kinetic studies require an efficient method of obtaining a quantitative measurement of progressive alignment, *in-situ* with high time resolution. Rheological characterization can provide the desired time resolution and can be measured in real time, but it is not sensitive to the structural changes^{26,41,49,51,52,63,73}. For example, the effective dynamic moduli can be measured simultaneously during shearing; but it is not yet possible to relate them to

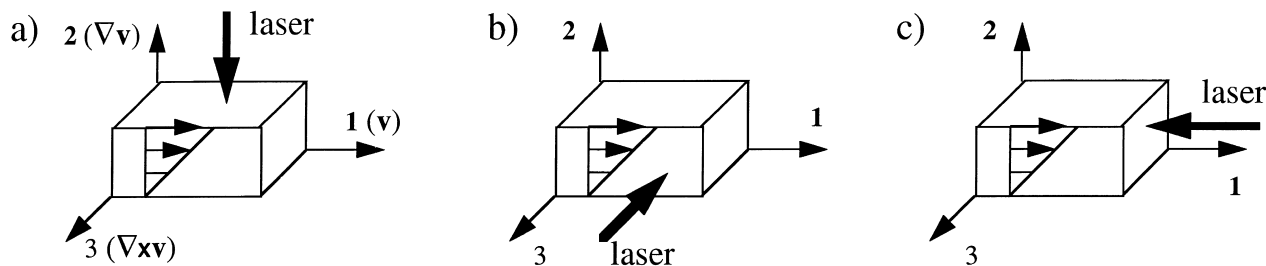


Figure 4 Notation for the birefringence measured by sending a polarized laser beam along three directions: (a) 1,3-birefringence, (b) 1,2-birefringence, and (c) 2,3-birefringence

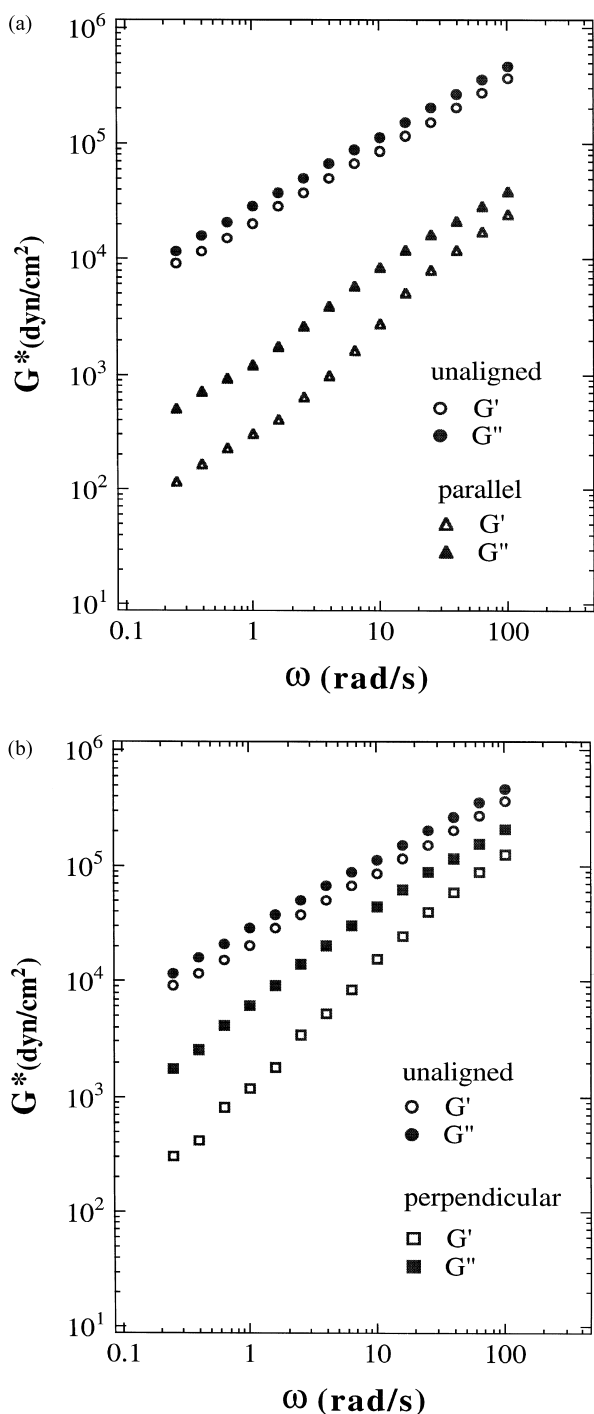


Figure 5 The storage and loss moduli of the unaligned and aligned states for a PS-PI (10K-10K) diblock copolymer⁶³: (a) unaligned and parallel aligned, (b) unaligned and perpendicular aligned. Note that the parallel orientation has the lower modulus, even at frequencies in Regime I

the orientational order, since a given value can correspond to many microstructural states⁴⁹. Conversely, a given alignment trajectory does not always have the same rheological signature. For example, it has been suggested that subtle changes in the loss tangent ($\tan \delta$ ranging from 0.85 to 1.2) can be used to track progress along the Regime III alignment trajectory⁵⁵. However, the small dip and subsequent increase observed in that sample are not observed in the other very similar PS-PIs along the Regime III trajectory^{49,72}.

Introduction of *in-situ* rheo-optical measurements during flow provided the desired time resolution (as fast as 10 ms) to probe the microstructural evolution during shear. Birefringence, which is sensitive to the degree of alignment and is correlated to the orientational order of BCP morphologies that have anisotropic optical properties (e.g. lamellae and cylinders), represents a reasonable choice for real-time kinetic studies. The interpretation of the transient birefringence for systems in which the microphases have significantly different refractive indices (form birefringence \gg intrinsic birefringence)^{49-51,63,76,77} and systems with microphases having nearly equal refractive indices (intrinsic birefringence \gg form birefringence)^{46,77} has been described. For systems that have sufficiently low birefringence, measurements can readily be made along two or potentially all three axes of the flow geometry (*Figure 4*). When the birefringence is large, the optical path must be kept small to avoid the retardation going over more than a few orders. In this case, complete characterization of the refractive index tensor could be performed using multiple beams at oblique angles with respect to ∇v ^{78,79}. While flow birefringence has the advantage of speed and the ease of sending a laser beam through multiple axes of a flow cell, compared with SAXS and SANS it has much lower information content. Instead of revealing the shape of the orientation distribution, birefringence is only sensitive to the second moment of this distribution. Information on possible flow-induced distortion of the nanostructure that is revealed in the wave-vector dependence of SAXS and SANS cannot be obtained from birefringence measurements. Further, interpretation of the birefringence results requires attention to the possible depolarization of light due to the polydomain structure in unaligned⁸⁰ and partially aligned⁷⁸ materials. Awareness of the relative magnitudes of the form and intrinsic contributions to the birefringence is required when interpreting flow birefringence when the deformation rate is high enough to perturb chain conformation⁴⁶. Like scattering measurements, a birefringence measurement made along only one axis is insufficient to characterize orientation^{2,49-51,63}. Thus, one needs to confirm the interpretation of the optical data using structural characterization by scattering and/or microscopy.

To achieve high time resolution and complete information on both the orientation distribution and domain structure that correspond to a given point along the path to alignment, it is natural to combine the individual methods that have these strengths. In this spirit, recent studies have used *in-situ* flow birefringence for its speed, *ex-situ* SAXS along velocity, velocity gradient and vorticity axes for its ability to reveal the shape of the orientation distribution, and *ex-situ* TEM along all three directions (\mathbf{v} , $\nabla\mathbf{v}$ and $\nabla \times \mathbf{v}$) to view the texture. This new approach has provided insight into the microstructural character of the 'fast' and 'slow' processes along the three types of alignment trajectories in Regimes I, II and III^{2,63}. The success of this experimental approach motivates future studies that combine an *in-situ* probe (flow-birefringence, SAXS or SANS), with *ex-situ* scattering along three axes (SAXS or SANS) and electron microscopy along three axes (TEM or FE-SEM).

Characterization of well-aligned states

Developing reliable methods to characterize well-aligned nanostructures is crucial, since the degree of order and density of defects can strongly affect the performance of well-aligned functional materials. TEM and other microscopic techniques provide the ultimate methods for observing the microstructures in a block copolymer^{26,41,42,44,45,53,54,73-75}. The lamellar dimensions and their directional distributions can be measured by the intensity distributions in the $(\nabla\mathbf{v}, \mathbf{v})$, $(\nabla\mathbf{v}, \nabla \times \mathbf{v})$ and $(\mathbf{v}, \nabla \times \mathbf{v})$ -planes using small-angle X-ray or neutron scattering experiments^{2,26,39-42,45,48,63}. Observations of birefringence in the $(\nabla\mathbf{v}, \mathbf{v})$, $(\nabla\mathbf{v}, \nabla \times \mathbf{v})$ and $(\mathbf{v}, \nabla \times \mathbf{v})$ planes can also provide a quantitative measure of the degree and direction of alignment⁷⁶. Rheometry is the least sensitive method for determining whether a single-crystal-like state has been reached; however, rheometry can give a rough idea of the alignment direction in some systems (*Figure 5*), if the correspondence between mechanical properties and microstructure has been previously established by scattering or microscopy. Therefore, electron microscopy is the only method capable of determining whether the alignment is 'perfect' (i.e. not only aligned, but also nearly defect-free). Complementary methods, such as SAXS, SANS and birefringence are able to quantify progress toward an aligned state and to detect when the BCP is *not* well-aligned.

Here we use the term 'well-aligned' only in reference to samples that have sharp peaks in their scattering patterns and uniform layers in TEM (*Figure 11*, point F)⁶³. Unfortunately the terms 'aligned' state and 'pure' state have been used in the literature in reference to transient states that are, in many cases, far from a well-aligned state^{41,42,44,45,47,48,52,55-58}. For example, the 'pure transverse state'⁵⁵ reported previously, when viewed in context, seems to be a weakly anisotropic transient state at the early stage of the parallel alignment trajectory at the very high frequencies (between points I and A on a Regime III trajectory, *Figure 6c*)⁶³. Indeed, there are many structures with strong unimodal scattering that are transient states along the way to a well-aligned structure as indicated by *in-situ* birefringence and SAXS (e.g. points C of *Figure 6*)^{2,63}. Verified by TEM micrographs, we have shown that a strongly perpendicular state corresponds to a saturated high value of 1,3-birefringence (*Figure 4*) close to a theoretical one for a monodomain state (indicated by the value marked F on the right-hand side of the graph in *Figure 6a*)⁵⁰. Using SAXS and TEM we have also shown that a well-aligned

parallel state is achieved when the 1,3-birefringence returns to zero^{2,50,63}. The birefringence has proven to be a much more sensitive indicator of a final well-aligned state than are the rheological properties.

TRAJECTORIES, KINETICS AND STRUCTURAL EVOLUTION

Trajectories of alignment

Three-dimensional mapping (*Figure 1*) provides a basis for viewing the alignment behaviour in terms of three parameters: temperature, frequency and strain amplitude. Qualitative aspects of the pathway leading to each alignment can also be represented on such a plot (e.g. the change in character of trajectory to the parallel state between Regimes II and III). However, this representation cannot capture the rich information on how alignment occurs that is manifested in the additional dimension of time. The evolution of structure during shearing provides direct information on the mechanisms of alignment, which gives insight into the origin of the frequency and temperature regimes associated with distinct orientation tendencies.

The pathways to distinct aligned states consist of a cascade of processes. At fixed frequency, temperature and strain amplitude, the character of the processes changes significantly with time. Qualitatively, this change in alignment dynamics as alignment proceeds can be rationalized as a consequence of the coarsening of the domain structure and the change in orientation distribution of the lamellae. Within a given frequency regime, flow alignment follows a characteristic path; we refer to this as a 'family of trajectories' along the time dimension. Three different families of trajectories have been identified (see footnote on p. 4680): one family of trajectories of perpendicular alignment in Regime I, and two different families of trajectories towards parallel alignment in Regimes II and III^{2,49,50,63}.

Comprehensive studies have been made to identify flow alignment trajectories in different frequency regimes by rheo-optical methods⁴⁹⁻⁵¹. Typically, within Regime I, the 1,3-birefringence increases steadily and finally reaches a saturated positive value during shearing (*Figure 6a*). There are two different signatures of parallel alignment: one with transient positive 1,3-birefringence (Regime II, *Figure 6b*), another with transient negative 1,3-birefringence (Regime III, *Figure 6c*). These distinct optical signatures indicate different transient states of microstructures for these three alignment trajectories. In the boundary between Regime I and Regime II (at $\omega \approx \omega_c'$), the direction of alignment depends on strain amplitude: below a particular strain amplitude γ_c , perpendicular alignment is induced along a trajectory similar to that shown in *Figure 6a*; above γ_c , the final orientation is parallel through a trajectory similar to that shown in *Figure 6b*; at γ_c , a novel trajectory has been identified recently⁷². During the alignment process at this specific condition ($\omega = \omega_c$ and $\gamma_o = \gamma_c$), the 1,3-birefringence increases rapidly to a transient peak value and drops gradually, in a manner similar to that seen for the 'fast process' and first portion of the 'slow process' of trajectory II (*Figure 7*, from point I to point M). Then the 1,3-birefringence increases steadily to a saturated value (much greater than the transient peak value) in a manner similar to that seen for trajectory I, and leading to perpendicular alignment (from point M to F) (*Figure 7*).

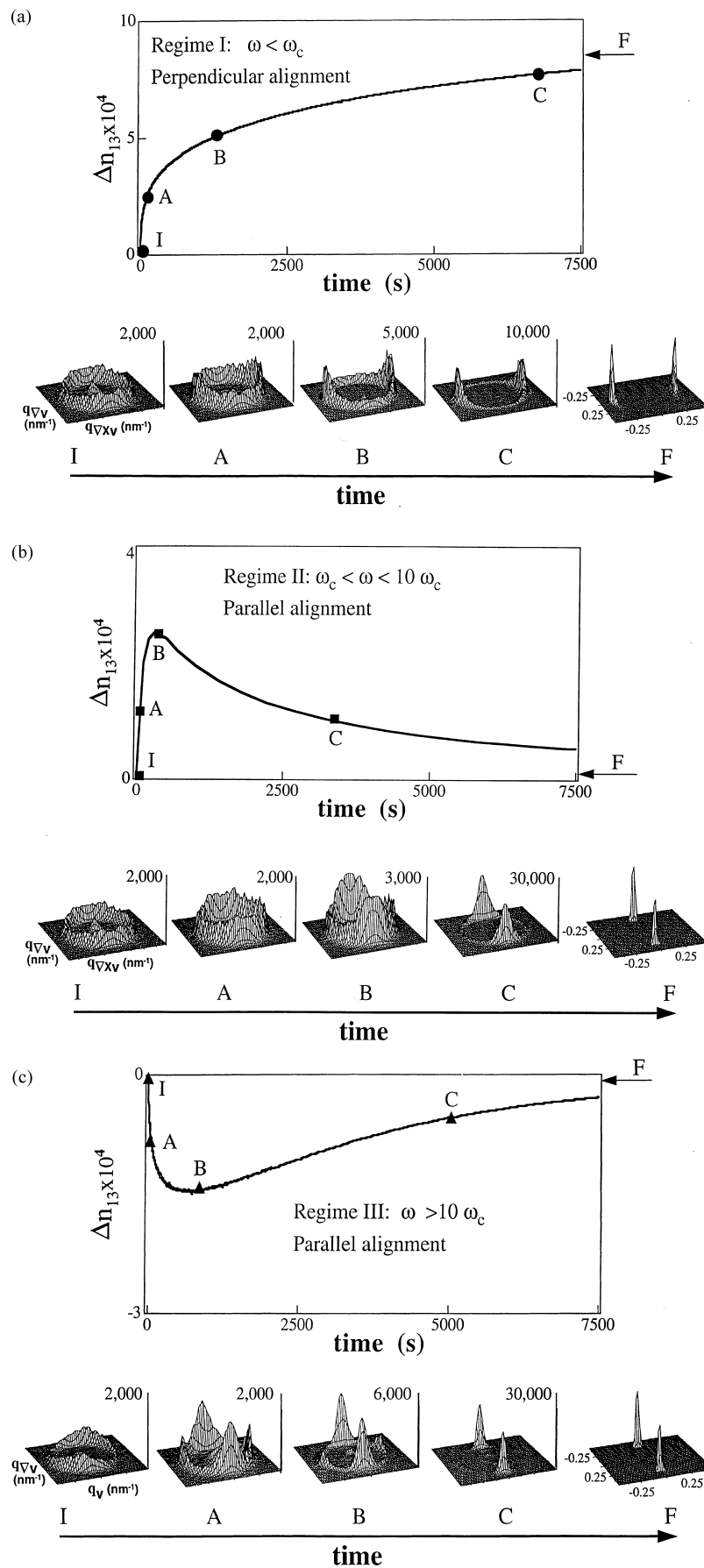


Figure 6 Three families of alignment trajectories are observed for a PS-PI (10K-10K) diblock copolymer⁶³ that has been heated through the ODT to erase its thermal and flow history, then cooled to a particular temperature in the ordered state where flow-induced alignment is performed. (a) Regime I route to perpendicular, (b) Regime II route to parallel, and (c) Regime III route to parallel (see Figure 1 for the range of temperatures, frequencies and strain amplitudes over which each type of alignment trajectory is observed)^{2,49,51,63}. One optical trace and a series of five SAXS patterns for each regime are shown: initial ordered but unaligned state (I); middle of the fast process (A); the transition from fast to slow processes (B); middle of the slow process (C); and the final well-aligned state (F)⁶³

A positive 1,3-birefringence en route to parallel alignment could be interpreted as indicating the existence of transient parallel and perpendicular orientations⁴⁹; *ex-situ* SAXS confirms this interpretation and shows that the orientation distribution contains all orientations between parallel and perpendicular, but not transverse⁶³. A transient negative 1,3-birefringence indicates that more transverse layers exist than perpendicular ones⁴⁹. This negative birefringence has been shown to correspond to the coexistence of transverse layers and parallel layers as transient states on the way towards parallel alignment, manifested in four-spot patterns revealed by *ex-situ* SAXS^{2,55,63} (Figure 6c). In fact, the evolution of the four-spot pattern with shearing time and strain amplitude⁵⁵ corresponds nicely to the birefringence's dependence on these parameters⁵⁰ (Figure 8). Since it is not straightforward to rescale the time or strain amplitude to account for the differences between the two BCPs studied by Gupta *et al.*^{49,50} and Zhang *et al.*⁵⁵, exact matching of the two sets of results is difficult. The correspondence indicated in Figure 8 is a qualitative one; in contrast, a direct correspondence is established by an integrated approach that combines rheo-optical measurements with *ex-situ* structural characterization (Figure 6a,b,c)^{2,63}.

The remainder of this section describes what is known about the kinetics and microstructure evolution of each of the three families of trajectories in Regimes I, II and III. These facts lay the groundwork for an up-to-date examination of current concepts regarding alignment mechanisms in the **Alignment Mechanisms** section.

Kinetics of alignment

The kinetics of alignment are of practical importance, since they provide the basis for estimating the processing time needed to harvest a well-aligned state, or a particular transient state, such as a bimodal parallel-transverse structure. The kinetics are also of fundamental importance, since they give clues regarding the mechanisms of alignment. Many factors, including shearing conditions (temperature, shear frequency and strain amplitude), and material properties (e.g. order-disorder transition temperature T_{ODT} , glass transition temperatures of each micro-phase, degree of entanglement and characteristic frequency ω_c') affect the alignment kinetics. Some of the most important thermodynamic and dynamic conditions can be parameterized using dimensionless groups, such as the strength of segregation ($\sim T/T_{ODT}$), the chain mobility ($(T/T_g)_A, (T/T_g)_B, (M/M_e)_A, (M/M_e)_B$), and the viscoelastic contrast between the layers ($T_{g,A}/T_{g,B}$). Shearing frequencies can be made dimensionless using a relevant characteristic relaxation timescale of the chains, or nanostructure, or domains. The choice of ω/ω_c' as a dimensionless frequency appears to be particularly significant since $\omega/\omega_c' \approx 1$ coincides with the boundary between Regimes I and II.

Shear conditions other than frequency (such as strain amplitude^{51,58}) affect the alignment trajectory; the region in (ω, T, γ_0) , space associated with a given type of trajectory is referred to as an 'alignment regime'. Within a particular alignment regime, changes in alignment conditions such as ω, T and γ_0 do not alter the direction of alignment. But these parameters affect the rate and sometimes ultimate degree of alignment⁵⁰. Usually the rate of alignment increases with frequency, temperature and especially strain amplitude^{49,50,63,72}.

Rheo-optical methods have been successfully used to characterize the kinetics of alignment of PEP-PEE⁴⁶ and

PS-PI (Figure 9)^{49,51,63}. For PS-PI within Regime I, in the early stage of alignment (point I to B in Figure 6a), 1,3-birefringence increases more rapidly than in the later stage of alignment (point B to F in Figure 6a). This could indicate that, during the course of shearing, there is a transition in the character of alignment, as though one process overtakes another in importance. To test this idea, the experiment is repeated with different strain amplitudes. Higher strain amplitude results in much faster overall alignment. In the initial 'fast process' from point I to B in Figure 6a, the kinetics speed up more strongly with strain than those of the later 'slow process' from point B to F. The effect of strain on the timescale of the development of alignment is highly non-linear: the time scale decreases as γ_0^{-3} at the initial 'fast process' (Figure 9b)^{49,63}. It is difficult to scale the late stage of alignment though, since the effects of strain amplitude are much weaker in the subsequent 'slow process'.

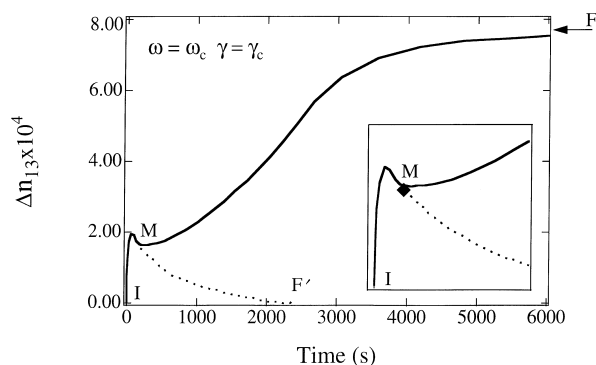


Figure 7 A novel trajectory in the boundary between Regimes I and II at a specific shearing condition: $\omega = \omega_c$ and $\gamma_0 = \gamma_c$. The first half of the trajectory (from I to M) is similar to those in Regime II; the second half (from M to F) follows the path similar to those in Regime I. The dashed line (from M to F') represents the path followed to parallel alignment when γ_0 is slightly greater than γ_c , all other conditions held fixed (from I to M, and to F')

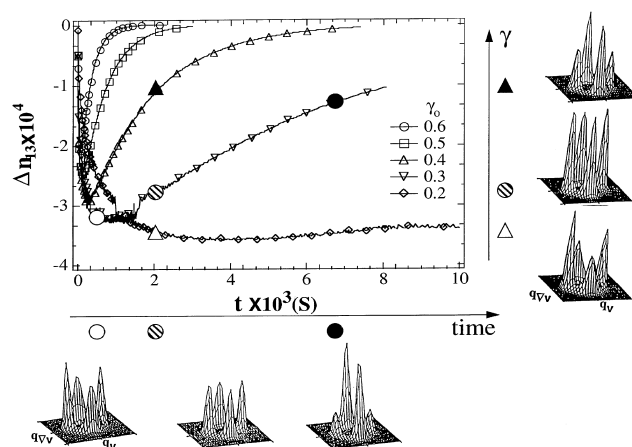


Figure 8 Comparison of the real-time optical^{49,51} measurements with *ex-situ* SAXS results⁵⁵ reveals the similarity in alignment behaviour of two different PS-PI samples. The SAXS patterns on the right-hand side illustrate the effect of strain amplitude ($\gamma_0 = 0.17, 0.33, 0.42$) for fixed shearing time (2 h); and the bottom SAXS patterns represent the time evolution (40 min, 2 h, 8.5 h) of structure at a given strain amplitude ($\gamma_0 = 0.30$). Analogous points are marked in the 1,3-birefringence traces using the symbols shown beside each SAXS pattern. The time evolution of SAXS patterns and their strain amplitude dependence resemble those manifested in the flow birefringence, even though SAXS results are for a polymer that is entangled with an inaccessible ODT while the birefringence results are for a PS-PI that is unentangled with accessible ODT

Within Regime II, the 1,3-birefringence increases very quickly early in the alignment process (point I to B in Figure 6b) and then decreases slowly (point B to F in Figure 6b). As expected, the overall alignment process speeds up with increasing strain amplitudes. The strain effect is stronger during the early stage of the process ('fast process'): the time needed to reach the transient peak value of Δn_{13} decreases as γ_0^{-5} (Figure 10a). During the subsequent 'slow process', the transient decay of 1,3-birefringence from the peak superimposes if time is rescaled by γ_0^{-5} (Figure 10b)⁵¹. These changes in scaling signal a difference in mechanisms of alignment between the initial fast process and the later slow process. Within Regime III, a change in character of the alignment mechanism is again indicated by the different strain dependence of the initial fast process and subsequent slow process^{50,63}. Unfortunately, it is impossible to tell what these different mechanisms are from birefringence measurements alone. Information on structure evolution during the 'fast process' and 'slow process' in each alignment regime (I, II and III) can uncover the nature of each process, as described in the next section.

Structural evolution

Detailed information on structural evolution is a prerequisite to understanding the mechanisms of the alignment processes regarding (1) the distinct families of trajectories, and (2) the nature of initial 'fast processes' and subsequent 'slow processes'. Here we briefly discuss previous work regarding the microstructure and defects in the initial unaligned and final well-aligned states. Structure development during the alignment process is discussed in the

context of the strengths and limitations of various experimental methods. Then structural evolution is described along three families of trajectories (I, II and III).

Microstructures of BCPs in the initial unaligned state are very different from those in the final well-aligned state. Prior to applying shear flow, quenched⁶³ or solvent casted⁴¹ samples appear to have a poorly organized, polydomain structure. Almost 70% of the material can exhibit a 'pebbly' texture in which the density of defects is so high that the lamellar morphology is obscured^{41,2}. The remaining material appears lamellar, but with a high concentration of various defects, including partially formed focal-conics^{41,63}. SAXS patterns from such materials show uniform rings in three orthogonal directions, and there are no preferential lamellar orientations. In a well-aligned sample, lamellae are well defined and highly oriented. Few types of defects exist and the defect density is much lower than in the unaligned state^{41,54,63}.

Regarding the structure evolution during shear processing from the initial unaligned state to the final well-aligned state, Zhang and Wiesner⁵⁵ have reported a particularly interesting progression of X-ray scattering patterns with shearing time. The results revealed the transient appearance and disappearance of a bimodal orientation distribution with coexisting parallel and transverse orientations, suggesting a dynamic context for interpreting four-spot patterns observed by Hashimoto *et al.*⁴⁵ (*in-situ*) and Winey *et al.*⁵². It also suggested the shape of the orientation distribution that might

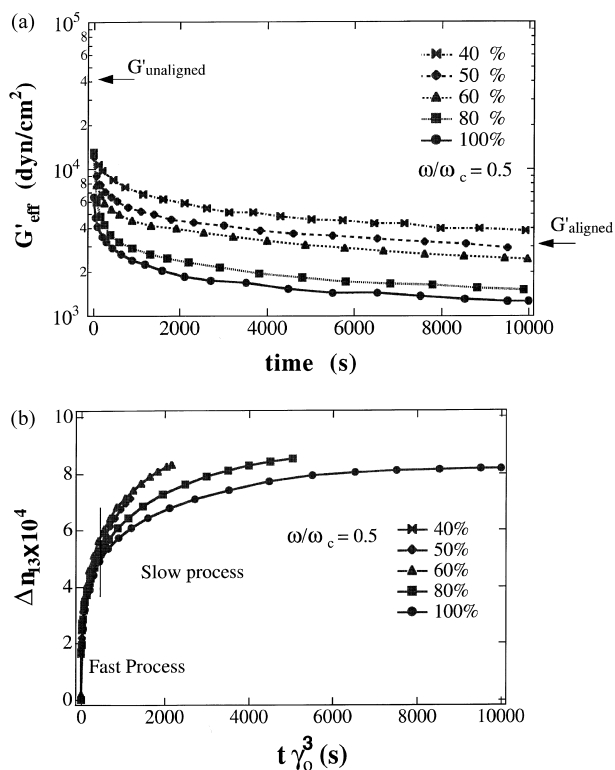


Figure 9 Rheo-optical monitoring of the perpendicular alignment process by oscillatory shearing at low frequency Regime I ($\omega < \omega_c$): (a) Effective storage modulus drops quickly at the beginning and remains almost constant afterward, and is not sensitive to the degree of alignment. (b) Birefringence increases steadily during the process, and the effect of strain is shown as a third power law in the initial fast process. A PS-PI (10K-10K) diblock copolymer was used⁶³

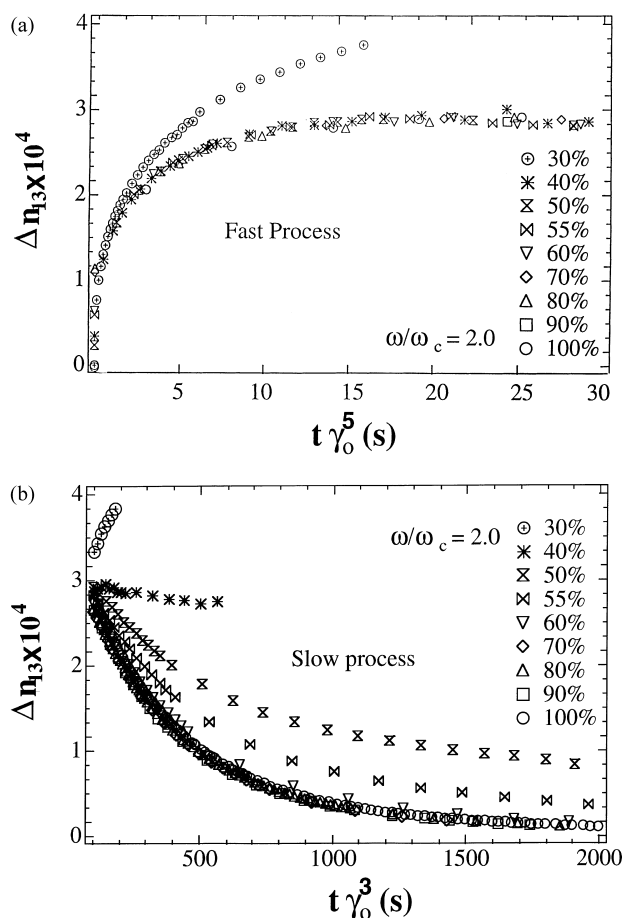


Figure 10 Kinetics of parallel alignment during oscillatory shearing at high frequency Regime II ($\omega > \omega_c$). The effect of strain amplitude is different for the initial (a) fast process from that in the subsequent (b) slow process, indicating the change of alignment mechanisms during alignment⁵¹

correspond to transient 1,3-birefringence results that indicated the appearance and disappearance of a strong transverse component en route to parallel alignment in Regime III (Figure 8)⁴⁹. However, it was not possible to connect the structural changes evident in the SAXS results with the rapid initial process and slow late-stage process that had been identified in Regime III^{49,50}. Further, it was difficult to recognize that these SAXS results pertained to one type of trajectory to parallel alignment (Regime III), but not to others (Regime II and IV). It was also difficult to recognize the similarity between behaviours of entangled, strongly segregated^{45,52,54,55} and non-entangled, weakly segregated^{49,63} systems. This is partly a consequence of the difficulty of performing a comprehensive *ex-situ* survey of the transient structure for many flow conditions in the three-dimensional space (T , ω , γ_0) for multiple samples. Without this broader perspective to guide the interpretation, it was possible to overly confine the relevance of the results in terms of materials (i.e. restricted to entangled, strongly segregated materials) and to over-generalize their relevance in terms of flow conditions (i.e. generalizing to all paths to parallel alignment). Such misunderstandings are hard to avoid unless *ex-situ* studies are linked to comprehensive *in-situ* results that guide the selection of sampling conditions.

Comprehensive rheo-optical measurements can provide an overall perspective on the range of alignment behaviours that occur as functions of the processing conditions. This perspective can allow one to select one particular set of conditions (ω , T) that is representative of a whole alignment regime. Extensive rheo-optical results on the effect of strain amplitude can guide the selection of a particular value of γ_0 to use to prepare samples for *ex-situ* electron microscopy and scattering measurements: the choice of γ_0 should be large enough to give a trajectory that leads to a well-aligned state, but small enough that the kinetics are sufficiently slow that they can be interrupted at desired stages of the alignment process, even in the initial fast process. Finally, rheo-optical measurements guide the selection of the points in time when samples should be taken for *ex-situ* characterization: they can record the point along the trajectory at which the sample was taken, as well as monitoring the relaxation of structure upon cessation of shearing and during subsequent cooling (or heating) to ambient conditions. Thus, while an optical observable like birefringence may not itself provide detailed structural information, it can be a powerful tool to guide *ex-situ* structural characterization.

A comprehensive approach that combines real-time birefringence measurements and *ex-situ* SAXS and TEM revealed the structural evolution during flow-induced alignment of a model diblock copolymer (PS-PI) in different alignment regimes (I, II, III)^{2,63}. In the initial unaligned state, the sample consists predominantly (roughly 70%) of poorly organized regions rather than well-defined layers. Layered domains exist with a variety of defect structures, including partially formed focal conics (Figure 11). Scattering results show that the initial structure is essentially isotropic (I in Figure 6a,b,c). During oscillatory shearing, the initial fast process in Regime III ($\omega_c \ll \omega$) is seen by TEM to be responsible for the formation of well-defined layers from poorly organized material (Figure 11), but the population of layers that is created is not isotropic, as shown by SAXS (Figure 6c). A bimodal distribution is produced by the 'fast process' in the very high frequency regime (Figure 6c). In the transition to the slow

process, the 1,3-birefringence indicates that the transverse population is at its maximum, representing the strongest bimodal character (parallel-transverse) that the system ever passes through on its way to parallel alignment. These transverse domains coexist with poorly organized regions and with approximately parallel regions containing 'chevron' bands (B in Figure 11), reminiscent of the images of transverse islands in a matrix of parallel material reported by Hudson for a lamellar diblock⁵⁴. The coarsening of the chevron pattern dominates the slow process, during which the transverse domains are also eliminated. Finally, a well-aligned state is achieved, as shown by sharp scattering patterns (F in Figure 6c) and uniformly aligned lamellae (F in Figure 11).

The same level of detailed information on structural evolution during flow-induced alignment has also been achieved for the families of trajectories in Regimes I and II^{2,63}. These two types of trajectories begin in similar ways in some respects, increasing the parallel and perpendicular projections and all orientations in between (Figure 6a,b from I to A to B). However, in the later stages the two trajectories are qualitatively different. The slow process in Regime I continues to increase the perpendicular projection, but progressively eliminates the other orientations (Figure 6a from B to C to F). In Regime II, the later 'slow process' reduces the perpendicular component of the orientation distribution as the parallel component becomes more and more dominant (Figure 6b from B to C to F).

By spanning the range of length and time scales involved, the cascade of structural changes was visualized: formation of layers from poorly organized regions; the creation, growth, coarsening and deformation of domains; the generation and elimination of defects, and the perfection of a well-aligned 'single-crystal-like' state. The body of results combining 1,3-birefringence, SAXS and TEM allows disparate observations^{45,49,52,54,55} to be viewed in a unified way^{2,63}. Such a clear picture of the evolution of flow-induced alignment processes is impossible to obtain from the transient rheo-optical results^{49,51} or from structural studies that do not have a context for relating the sample points to their corresponding positions along a given alignment trajectory^{45,52,54,55}. Without TEM, SAXS alone is not able to uncover the existence of poorly organized regions, their transformation into layers, the types of defects that emerge and how the defect texture coarsens. On the other hand, without SAXS, TEM alone is not well suited to giving a statistical distribution of layer orientations.

ALIGNMENT MECHANISMS

Towards the goal of predicting the direction, rate and degree of flow-induced alignment, many mechanisms have been put forward over the past two decades^{25,26,33-36,39-55,73}. Some concepts were proposed in an attempt to understand the selection of alignment directions, such as the orientation that has the 'minimum moduli'⁴⁷; some were dedicated to understanding the formation of aligned layers from isotropically distributed grains, such as 'domain dissolution' ('melting'), 'grain rotation'^{26,39,41,73} and 'irreversible rocking'⁴⁶; others were expected to explain both the direction and mechanism of alignment, such as 'selective melting'³⁹ and 'selective creation'^{2,63} of layers. Some authors explained particular alignment behaviours in terms of the material's characteristics, such as 'entanglement'⁵⁵, 'weak segregation'³⁹, 'strong segregation'⁵⁵, or

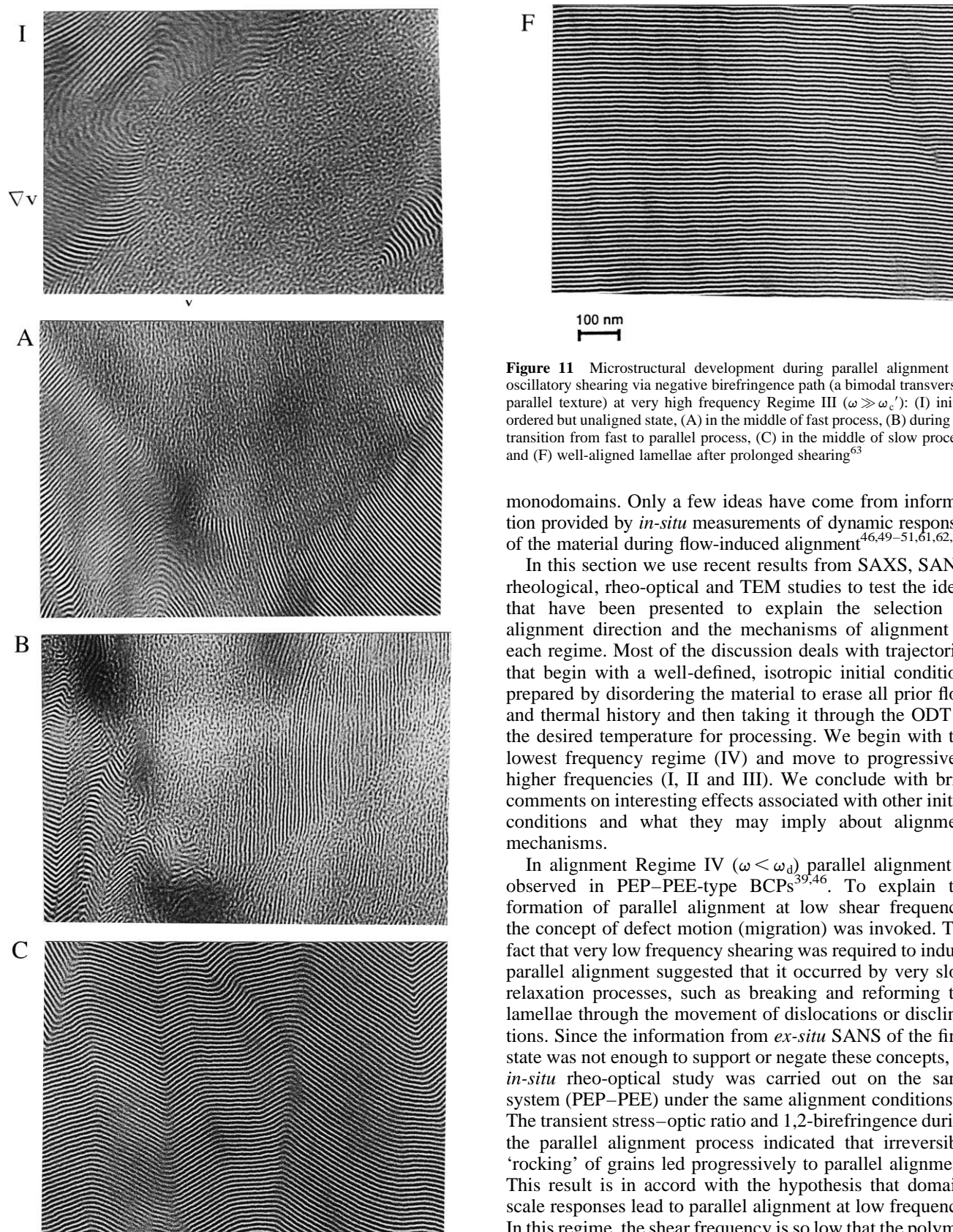


Figure 11 Microstructural development during parallel alignment by oscillatory shearing via negative birefringence path (a bimodal transverse-parallel texture) at very high frequency Regime III ($\omega \gg \omega_c'$): (I) initial ordered but unaligned state, (A) in the middle of fast process, (B) during the transition from fast to parallel process, (C) in the middle of slow process, and (F) well-aligned lamellae after prolonged shearing⁶³

monodomains. Only a few ideas have come from information provided by *in-situ* measurements of dynamic responses of the material during flow-induced alignment^{46,49–51,61,62,81}.

In this section we use recent results from SAXS, SANS, rheological, rheo-optical and TEM studies to test the ideas that have been presented to explain the selection of alignment direction and the mechanisms of alignment in each regime. Most of the discussion deals with trajectories that begin with a well-defined, isotropic initial condition, prepared by disordering the material to erase all prior flow and thermal history and then taking it through the ODT to the desired temperature for processing. We begin with the lowest frequency regime (IV) and move to progressively higher frequencies (I, II and III). We conclude with brief comments on interesting effects associated with other initial conditions and what they may imply about alignment mechanisms.

In alignment Regime IV ($\omega < \omega_d$) parallel alignment is observed in PEP-PEE-type BCPs^{39,46}. To explain the formation of parallel alignment at low shear frequency, the concept of defect motion (migration) was invoked. The fact that very low frequency shearing was required to induce parallel alignment suggested that it occurred by very slow relaxation processes, such as breaking and reforming the lamellae through the movement of dislocations or disclinations. Since the information from *ex-situ* SANS of the final state was not enough to support or negate these concepts, an *in-situ* rheo-optical study was carried out on the same system (PEP-PEE) under the same alignment conditions⁴⁶. The transient stress-optic ratio and 1,2-birefringence during the parallel alignment process indicated that irreversible 'rocking' of grains led progressively to parallel alignment. This result is in accord with the hypothesis that domain-scale responses lead to parallel alignment at low frequency. In this regime, the shear frequency is so low that the polymer chains and lamellae are fully relaxed; thus, shearing only deforms the domains and disturbs the defects between them. The microstructural dynamics that control parallel alignment at these low frequencies appear to be sensitive to the differences between PEP-PEE-type and PS-PI-type lamellae. Parallel alignment Regime IV is consistently observed in PEP-PEE-type polymers; however, in PS-PI-type systems, perpendicular alignment behaviour generally

'viscoelastic contrast'⁴⁷. A few proposed mechanisms were confirmed by experimental observations such as 'defect migration', 'selective creation' and 'selective elimination'; but many of them have not yet been validated. Arguments regarding the selection of alignment direction have been based primarily on the relative stability of different

persists to the lowest accessible frequencies^{47,49,50}, unless the ordered sample is subjected to a particular pressing and annealing treatment prior to shearing.

As shear frequency increases, oscillatory shear may couple with the dynamics of the nanostructure (lamellae). In Regime I ($\omega_d < \omega < \omega_c'$) perpendicular alignment can be induced (in both PEP-PEE-type and PS-PI-type BCPs). In PEP-PEE, this represents a flip in orientation around ω_d . To explain this phenomenon, it was suggested that fluctuations play a role in selective melting, making the perpendicular orientation the least susceptible to shear-induced disorder. This concept provided a hypothesis regarding the selection of one direction over another as a function of frequency and temperature: perpendicular alignment would be selected at frequencies that couple to lamellar dynamics and at temperatures close to T_{ODT} ^{39,55}.

The evidence that selective melting causes perpendicular alignment is indirect. The detailed structural evolution observed during the perpendicular alignment process^{2,63} provides an opportunity to re-evaluate this concept. If selective melting were playing an important role, it could be expected to dominate during the early stage of the alignment process when the amount of unfavourably oriented material is the greatest. One would expect an initial rapid growth of the perpendicular component, while other orientations would be depleted (or left unchanged). Instead, SAXS results show that the initial process does not select perpendicular alignment over parallel—it enhances both of these, as well as all orientations between the two (*Figure 6*). Further, electron micrographs show that the initial enrichment of this range of orientations occurs by a process that converts poorly organized regions into well-defined lamellae, suggesting a mildly 'selective creation' of layers with a range of orientations instead of a strongly 'selective melting' leading to a specific one. The selection of the perpendicular orientation occurs during the subsequent slow process as 'selective elimination' occurs^{2,63}. It is unlikely that shear-induced melting plays a role in the late stage processes, since the most unstable orientations have been eliminated and the material has become relatively homogeneous, so that localized melting is decreasingly plausible (and the energy involved in shearing is too low to cause bulk melting).

While the exact mechanisms are still not clear, the formation of well-defined layers during the fast process may involve defect dynamics such as the elimination of partially formed focal conic defects and, possibly, the rotation of the local phase-segregated structure within the poorly organized regions. The selectivity that is observed during the initial process in Regime I may be a consequence of the symmetry of oscillatory shear combined with the long time scale of the deformation—longer than the single chain relaxation time, long enough to allow relaxations on the scale of the whole chain or even the nanostructure. By symmetry the only orientations that can be progressively reinforced by oscillatory shearing are those that are affected the same way by forward and reverse cycles, i.e. those with fore–aft symmetry. These relaxations can produce out-of-plane reorganizations of structure that avoid higher energy distortions in the plane (such as the creation of transverse layers). All of the other orientations that have fore–aft symmetry are enhanced. From the orientation distribution created by the initial fast process, the slow process winnows out all but the perpendicular alignment by 'selective elimination'. This process takes place after layers and domains are clearly defined in the TEM images; thus, the

selectivity of the slow process may involve dynamics at the scale of whole grains.

Moving up in frequency to the boundary between Regimes I and II, in the vicinity of ω_c' , the selection of alignment can be 'flipped' from perpendicular to parallel at fixed conditions of frequency and temperature simply by increasing the strain amplitude⁵¹. Based on the concept that shear distorts fluctuations and causes selective melting, followed by ordering into perpendicular layers, higher strain amplitude should lead to stronger and more rapid perpendicular alignment, due to greater distortion of the fluctuations. Instead, increasing γ_0 leads to parallel alignment. This suggests that the mechanisms for perpendicular and parallel alignment coexist, and that the strength of the parallel mechanism increases more rapidly with strain amplitude than that of the perpendicular mechanism. As the underlying processes that lead to each alignment become better defined, models of their kinetics may capture this difference in their strain-dependence. In turn, understanding the interplay of strain, frequency and temperature may explain the shape of the boundary surface in (ω , T , γ_0)-space that separates distinct alignment regimes.

As one moves fully from Regime I into Regime II by increasing frequency through ω_c' , the alignment tendency shifts to parallel for PS-PI-type lamellae^{42,47–50,63,72}, while no alignment has been reported in PEP-PEE-type polymers for $\omega > \omega_c'$. The most striking differences between the two systems are (1) that PS-PI-type materials have very different local friction in the distinct lamellae, while there is little 'viscoelastic contrast' in PEP-PEE-type systems, and (2) the PS-PI-type polymers that are typically studied are not well entangled, while the PEP-PEE-type polymers are highly entangled. Based on the first difference, it has been suggested that the mechanism for parallel alignment at $\omega > \omega_c'$ may require 'viscoelastic contrast'⁴⁷. If so, this hypothesis may also explain the reason the alignment tendency changes at ω_c' . At lower frequencies the response is controlled by the layers as a whole; it is insensitive to more local dynamics since the chains are relaxed. Above ω_c' , chain conformation is distorted and more local relaxation dynamics play a role; thus, non-uniform monomeric friction could be involved, flipping the alignment direction to parallel. Alternative explanations of the flip in orientation at ω_c' include the hypothesis that the system adopts the orientation that minimizes the dynamic moduli at the frequency of the applied shear⁴⁷ and the concept that parallel alignment is favoured at frequencies where the elastic character of the material dominates (relatively small $\tan \delta$)^{48,55,56}. While these ideas were inspired by the behaviour of some specific PS-PI materials, they fail for other very similar PS-PI lamellae, as illustrated in *Figure 12* and *Figure 3c*, respectively.

The mechanisms that have been suggested to explain parallel alignment have not distinguished Regimes II and III, since most of them were put forward before the qualitatively different pathways to parallel orientation above ω_c' were identified. We discuss the ideas that presume the transverse orientation is eliminated most rapidly in the context of Regime II, in which this assumption holds. Later we will discuss concepts that relate to the mechanism of alignment through transient states rich in the transverse orientation.

As a possible mechanism for forming parallel layers, it has been suggested that unfavourably oriented domains might be destroyed, then formed into parallel oriented lamellae^{25,26,41,55}. A closely related idea is that small

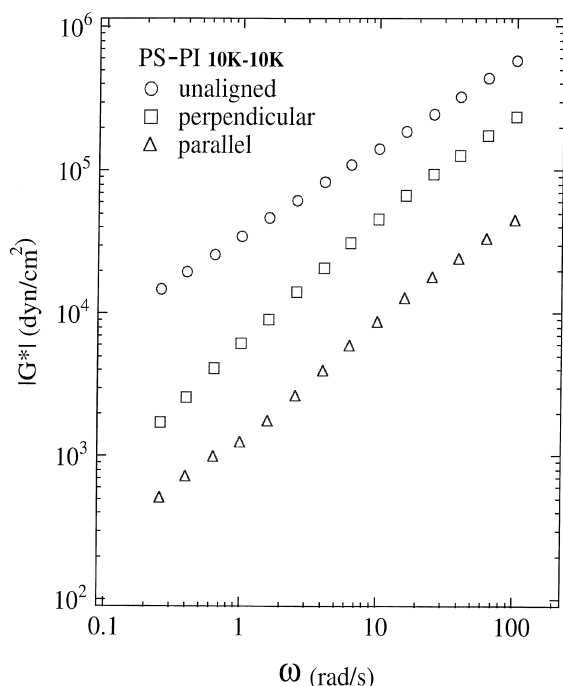


Figure 12 Linear complex dynamic moduli of unaligned, parallel and perpendicular aligned PS-PI diblock melts at 115°C. The absolute values of complex dynamic moduli are the lowest for parallel alignment in the whole range of frequency. ω_c' is about 2 rad s⁻¹ at this temperature⁶³

regions might be destroyed at any one time and converted progressively into parallel layers (partial dissolution of microdomains)^{26,41}. The shearing energy applied to the initial unaligned state has been estimated to be sufficient to destroy small microdomains⁴¹. Unfortunately, no method has been available to detect such destruction/reformation or domain dissolution (although recent fluorescence techniques⁸² would open the way to *in-situ* rheo-optical

probes of flow-induced disorder). Recent electron microscopy images of the evolution of microstructure with shearing in Regime II do show that poorly organized regions are progressively eliminated and well-ordered layers increase, especially during the initial fast process⁶³. This appearance is evocative of the destruction/reformation concept. However, the fast process does not lead to the selection of parallel alignment in particular; instead it enriches the whole range of orientations that are tangent to the flow direction (parallel, perpendicular and all orientations in between). The subsequent slow process in Regime II eliminates the perpendicular and intermediate orientations created during the initial fast process, but its mechanisms are not yet clear. A characteristic texture of sinuous defects oriented preferentially along the flow direction is established by the initial process. This larger-scale structure coarsens during the slow process. Thus, the mechanism of the slow process may involve larger-scale relaxations, such as defect migration.

The path to parallel alignment at very high frequencies (Regime III, $\omega \gg \omega_c'$) involves an initial fast process that is quite unique: a bimodal distribution that consists of parallel and transverse lamellae is created. This transient is so different from the one in Regime II that a distinct mechanism of parallel alignment must be responsible. Indeed, the concept of destruction/reformation in the literature would anticipate the most rapid destruction of the transverse component of the orientation distribution; some other mechanism must be at work to create the transverse/parallel texture. Based on the observation that this bimodal structure was evident in SAXS patterns for entangled PS-PI lamellar BCPs^{45,52,55}, it was suggested this orientation distribution resulted from an 'entanglement effect' and elongation of chains along the flow direction⁵⁵. However, the Regime III trajectory is observed for unentangled PS-PI's, and at such small strain amplitudes (as small as $\gamma_0 = 10\%$), that segmental orientation is hardly

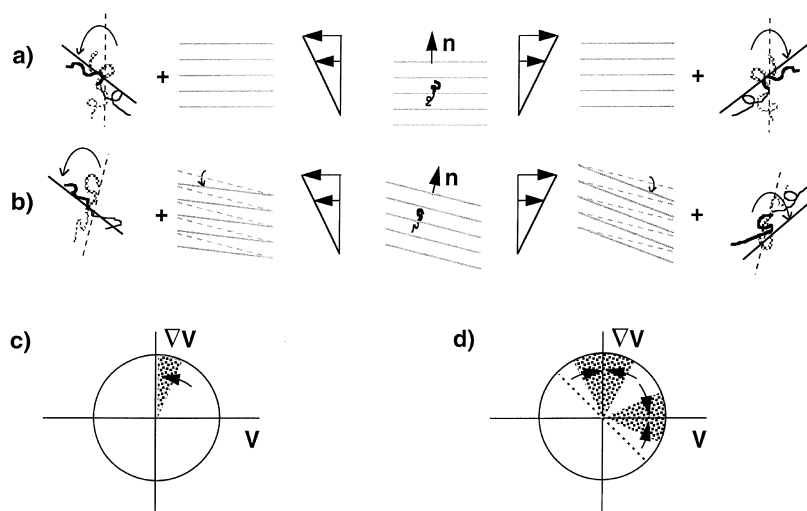


Figure 13 The role of chain distortion in the development of the bimodal transverse-parallel texture en route to parallel alignment at very high frequencies ($\omega \gg \omega_c'$) (Regime III). The extensional component of shear affects chain conformation as shown schematically by the solid chains (deformed) compared with the dotted chains (undeformed). Convection of the layers produces a reorientation indicated by the solid lines (deformed) versus the dotted lines (undeformed). (a) Parallel layers are affected the same way by forward and reverse cycles, so there is no tendency to reorient. (b) Layers tilted away from the parallel orientation are affected differently by forward and reverse cycles. If their normal \mathbf{n} is tilted to the right, then the distortion of the chains is stronger in the forward than in the reverse direction; consequently, the net effect of a full cycle is to promote reorientation toward parallel alignment. (c) Thus, layers with \mathbf{n} in the shaded sector on the right side of the $\nabla\mathbf{v}$ axis will tend to evolve toward parallel alignment ($\mathbf{n} \parallel \nabla\mathbf{v}$). (d) The same reasoning applies to orientations tilted in the opposite direction relative to parallel, so they will also tend to evolve toward parallel alignment (shaded region on the left side of the $\nabla\mathbf{v}$ axis). Similarly, orientations tilted away from transverse alignment would progressively rotate into transverse (shaded regions near the \mathbf{v} axis). Schematic diagrams regarding near-transverse layers have been shown elsewhere²

perturbed^{63,49,51}. (Furthermore, Regime III has not been reported in PEP-PEE-type polymers which are well entangled.)

Two very general concepts may explain the creation of the bimodal parallel-transverse texture during the fast process in Regime III². First, chain distortion may play a central role, since this texture has only been observed at shear frequencies so high the polymer chains are not able to relax ($\omega \gg \omega_c'$). Second, only orientations with fore-aft symmetry can be progressively reinforced by oscillatory shearing as explained earlier. If these two considerations are taken together, only two orientations might be induced by very high frequency shearing: parallel and transverse. The other orientations with the right symmetry have a projection along the perpendicular orientation, so they can only form through larger-scale relaxations that exchange material out of the shearing plane. The timescale of the deformation is too fast for these large-scale rearrangements to occur. This reasoning explains why transverse and parallel orientations could be enhanced, but does not explain why both are generated.

To explain the bimodal texture, a mechanism to generate both parallel and transverse layers during the fast process has been suggested. Two factors affecting the lamellar orientation due to shear are considered: the deformation of the layers and the distortion of chain conformation, as illustrated schematically in *Figure 13*. These effects can disturb the relative orientation of the chains with respect to the layers. Except for the special cases of parallel or transverse lamellae (*Figure 13a*), this disturbance is more severe for one direction of shearing than the other (*Figure 13b*); each half-cycle of oscillatory shear can affect the system differently, leading to a net reorientation. For example, consider layers that are near parallel alignment, i.e. having layer normal in the $(\nabla \mathbf{v}, \mathbf{v})$ -plane within $\pm 45^\circ$ of the velocity gradient direction. The half-cycle that would tend to rotate the layers away from parallel alignment also extends the chains more strongly away from the layer normal than the opposite half-cycle of shear (*Figure 13b*). The net effect of a full cycle will tend to rotate the layers toward parallel alignment (*Figure 13c*). For lamellae near transverse alignment, the asymmetry with respect to forward and reverse shear directions would progressively reinforce transverse alignment (*Figure 13d*). Thus, this mechanism can explain the enhancement of parallel and transverse components starting from an initially isotropic orientation distribution. Electron micrographs show that the growth of the bimodal orientation distribution occurs, while poorly organized regions are converted to well-defined layers. Indeed, a process that straightens out convolutions in the local structure would contribute to transforming poorly organized material into lamellae.

Simultaneous with the creation process that produced transverse and parallel domains, there should exist a mechanism that converts the unstable transverse domains to the more stable parallel orientation. This unspecified mechanism dominates the slow process, when most of the material exists in well-organized lamellae in either nearly transverse or nearly parallel orientations. One likely hypothesis is that the boundaries surrounding transverse domains tend to move progressively inward, leading to shrinkage and eventual disappearance of transverse regions. Electron micrographs also implicate defect migration in the refinement of the parallel alignment during the slow process. Tilt walls that are preferentially oriented normal to the flow direction separate regions that are somewhat

tilted up and down relative to parallel alignment. Images of the microstructure suggest that these boundaries tend to migrate in the direction of the more severely misaligned region; when two walls meet, they annihilate each other. The result is a simultaneous coarsening of the chevron pattern of defects and a tightening of the orientation distribution of the near parallel lamellae.

Reflecting on the trajectories of Regimes IV, I, II and III, it appears that the changes in the character of both the fast and slow processes as one moves from very low frequencies ($\omega < \omega_d$), through moderately low frequencies ($\omega_d < \omega < \omega_c'$) and moderately high frequencies (above, but near ω_c'), to very high frequencies ($\omega \gg \omega_c'$) can be qualitatively understood in terms of the changes in the relaxation processes that can occur on the timescale of the deformation. Certain general mechanistic concepts may be relevant in all regimes. For example, defect migration appears to be important in the slow process in all regimes. However, the specific defects involved, their anisotropic arrangement and their specific motions differ from one regime to the next and with position along a given trajectory. These individual characteristics may account for the differences among their kinetics as functions of processing conditions, such as the distinct non-linear effects of strain on kinetics.

Up to this point, we have been discussing alignment behaviours that have been observed as the structure evolves from an isotropic, ordered initial condition. In some cases, the behaviour appears to be insensitive to the precise initial condition. For example, the bimodal transverse-parallel texture has also been observed in PS-PI-type diblocks that have ODT so high that it cannot be reached to erase the flow and thermal history associated with sample preparation^{45,52}. Consequently, the initial condition is almost invariably somewhat anisotropic; in addition, a particular annealing procedure has been applied to some samples, but not others^{55,63}. In spite of these differences, the bimodal texture is produced by very high-frequency shearing in the various systems. On the other hand, some very interesting changes in behaviour as a function of initial condition have been discovered. Particularly in relation to the low-frequency regime of parallel alignment (Regime IV), it has been reported that PS-PI type polymers exhibit parallel alignment at low frequencies, but only if they are pressed and annealed first⁵⁶. This treatment is not a prerequisite for low-frequency parallel alignment in PEP-PEE-type polymers⁴⁶. It is not yet known whether the dominant effect is due to the flow history (pressing tends to induce parallel alignment), the thermal history or a particular combination of the two. A closely related phenomenon accessible only in PS-PI samples that have been pre-treated to exhibit low-frequency parallel alignment is another variation of strain-induced flipping: at frequencies that lie in Regime I, it has been reported that small strains produce parallel alignment, while higher strains induce perpendicular⁵⁸. It is not yet clear whether the parallel alignment that is generally present in pressed samples plays a role in this behaviour as well. Clarification of the physical origins of these alignment behaviours will very likely lead to new insights into the alignment mechanisms of Regimes I and IV.

Highly aligned initial conditions have been used to examine the potential for switching materials back and forth between distinct aligned states and to examine the dynamics of specific defects. Switching experiments have shown that in PEP-PEE-type systems, parallel alignment induced in Regime IV can be flipped to perpendicular by imposing

conditions that belong to Regime I; however, a perpendicular alignment cannot be flipped back to parallel by imposing conditions in Regime IV^{39,46}. On the other hand, in PS-PI-type lamellae, perpendicular alignment can be flipped to parallel by imposing conditions that lie in Regimes II or III; but the reverse transformation from parallel back to perpendicular cannot be produced⁵⁰. Well-aligned parallel samples have been used to study the motion of edge-dislocations by imposing compression on the sample and monitoring the subsequent stress relaxation⁵⁴. Nearly perfect parallel samples have been created using prolonged annealing after cessation of oscillatory shearing; the creation of tilt wall defects by oscillatory shear has been investigated⁵³. Fundamental understanding of specific defect types and their motions appears to be of central importance to a range of alignment mechanisms and these studies serve as models for future work in this area.

EFFECT OF MACROMOLECULAR ARCHITECTURE: BRIDGES AND LOOPS

Different macromolecular architectures affect chain conformation in microphase-separated block copolymers. Diblock copolymers, such as PEP-PEE and PS-PI types, have only one possible conformation, while ABA triblocks and ABC triblocks have more possibilities, such as bridges and loops (*Figure 14*). A_2B type¹⁸ and star block copolymers¹⁷ may have interesting packing behaviour due to asymmetric 'crowding' along interfaces in the ordered state. Thus, the effect of macromolecular architecture represents an important dimension in understanding flow-induced alignment. In this section, we will discuss ABA type and ABC triblock copolymers. Flow-alignment of other types of macromolecular architecture remains to be explored.

ABA triblock copolymers

Although ABA triblock copolymers self-assemble into morphologies similar to diblocks⁸³, their chain conformation is very different (*Figure 14*). Diblocks have their junctions tethered along the interface between A-rich and B-rich nanophases. On the other hand, ABA triblocks can adopt either a loop conformation with two ends in the same nanodomain or a bridge, with the two ends in different nanodomains on either side of the B-rich layer. The percentage of bridge conformations has been measured experimentally by dielectric relaxation⁸⁴ and evaluated by theory⁸⁵⁻⁸⁷.

It has been argued that the difference in flow alignment behaviour of ABA and AB copolymers results from the presence of bridging chains. Riise *et al.* compared the alignment behaviour of lamellar PS-PI and PS-PI-PS BCPs⁴⁴. Since they used a molecular weight of PS-PI-PS almost exactly twice that of an extensively studied PS-PI, the PS-PI-PS sample can be envisaged as two of these PS-PI molecules linked together at the isoprene ends. As described before, both parallel and perpendicular alignments were observed for the PS-PI diblock (*Figure 1*), but for the PS-PI-PS triblock, only perpendicular alignment was observed, even at frequencies above ω_c' . This was explained by the existence of bridges in the ABA triblock: in the parallel aligned diblock, the lamellae can easily slide past each other during shearing; while in the ABA triblock, sliding would be resisted by the bridges between adjacent layers. This was interpreted in terms of a decrease in viscoelastic contrast. Tepe *et al.* studied a PEP-PEE-PEP triblock⁷¹ and found that shearing in the ordered state

produced only parallel lamellae, even for $\omega_d < \omega < \omega_c'$. This behaviour is quite different from that of both the PEP-PEE diblocks³⁹ and the PS-PI-PS triblocks⁴⁴. Tepe *et al.* argued that since bridging increases the stiffness of the PEE block, viscoelastic contrast could be increased; thus, parallel alignment is preferred. Unfortunately, there is no experimental evidence that bridging changes the viscoelastic contrast of BCPs.

ABC triblock copolymers

In terms of the effects of bridging chain conformations, ABC triblock lamellae represent the upper limit: when strongly segregated three-phase nanostructures are formed, all chains must adopt a bridge conformation (*Figure 14*). At least two types of interface exist in ABC triblocks, while there is only one type of interface in the AB and ABA block copolymers. Thus, ABC triblock copolymers can assemble fascinating arrays of nanostructures⁸⁸⁻⁹⁴ that are impossible to form using either AB or ABA block copolymers. Many interesting new flow alignment phenomena are expected in such rich systems and need to be explored. For example, for hierarchical structures such as helical strands surrounding cylinders in a continuous matrix, one could envision shearing the material in a first step that aligns the cylinders along the velocity direction, followed by small amplitude shear at an angle oblique to the axis of the cylinders to select only one handedness of the helices.

To investigate flow phenomena in ABC triblocks, a model system has been designed for future research⁷². The three blocks in this model ABC system are styrene (S), isoprene (I) and a random copolymer of styrene and isoprene (R). This system has several advantages relative to the ABC triblocks that have received the most attention to-date (PS-PI-PVP, PS-PB-PMMA and PS-PEB-PMMA). For example, the blocks can be grown in any order (SIR, SRI or ISR)¹⁹, the relative magnitude of the interaction parameters can be tuned as a continuous variable by changing the styrene content in the random block, and the absolute magnitude of the interaction parameters can be tuned by partial hydrogenation of the isoprene units.

As a starting point, 'symmetric' ABC triblocks were

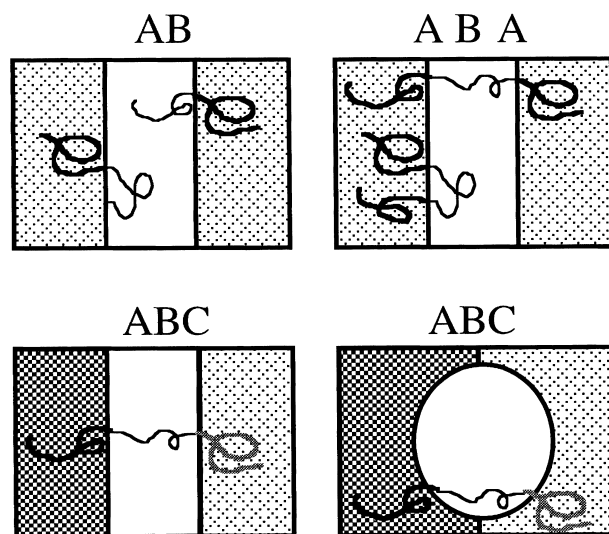


Figure 14 Chain conformations in AB diblock, ABA triblock, and ABC triblock copolymers. Only one type of interface (A-B) exists in both AB diblock and ABA triblock copolymers. ABA triblocks can form either bridges or loops. For ABC triblocks, only bridge conformations are allowed in three-nanophase-separated structures

prepared. They have the same lengths for all three blocks, and the same content of styrene and isoprene in the random block. Four overall lengths (approximately 15K, 20K, 25K and 35K per block, respectively) in all three permutations (RSI, SRI, RIS) are compared with each other. Here we summarize some preliminary results on the alignment behaviour of lamellar nanostructures⁷². Two-nanophase-separated lamellae (such as SRI-15, SRI-20, RSI-15 and SIR-20) and three-nanophase-separated lamellae (SIR-35, RSI-35 and SRI-35) are investigated. Most two-nanophase-separated lamellae (SRI-15, RSI-15) behave in a manner very similar to that of lamellar diblocks (*Figure 15*): they show three regimes of alignment (I, II and III), fast and slow processes along each trajectory, and strain-dependent kinetics like PS-PI diblocks. SIR-20 behaves like the SIS triblock: only perpendicular alignment is achieved below and above ω_c' . Actually, TEM micrographs of SIR-20 suggest that the two end-blocks S and R are miscible (i.e. like ABA-type triblock lamellae). Micrographs of RSI-15 suggest that two adjacent blocks S and R are miscible (like asymmetric AB diblock lamellae). TEM images of SRI-15 and SRI-20 imply that the middle block R is partially miscible with both S and R blocks, resembling a weakly segregated symmetric diblock lamella.

A new feature introduced to the lamellar system by ABC triblock copolymers is the occurrence of a new type of defect: three microphase lamellae with correlated perforations (*Figure 16*). The lamellae in SIR-35 consist of repeating stacks of [I-S-I-R]. The isoprene layers are observed to be continuous; however, the intermediate layers are composed of alternating sections of S and R. When there is S on one side of the I layer, there is R on the other side. Thus, the defects represented by an S/R boundary within a given layer are correlated with R/S defects on the layers just across the adjacent I layers. As these defects annihilate each other upon annealing, the structure coarsens, and long-range correlations produce striking patterns, including those that resemble a ship's wake. Analogous defects are observed in RSI-35, but with S as the continuous layers. However, these defects are not observed in SRI-35, in which all layers are nearly defect-free. A possible explanation has been proposed for the formation of these defects at an order-order transition from two-nanophase to three-nanophase segregation. If the two-phase precursor has layers that are rich in the mid-block (B) segregated from layers in which the end blocks are mixed (A/C), then the transition to the three microphase structure will tend to occur by the lateral segregation of A from C, leading to the correlated perforations. If the two-phase precursor has layers rich in the respective end blocks with the mid-block mixed in one or both of the layers (i.e. (A/B)-(B/C) or A-(B/C) or (A/B)-C), then segregation into three layers can occur without any tendency to form this type of defect. These early studies represent the first step towards developing new processing strategies for ABC triblock copolymers⁷².

IMPLICATIONS AND FUTURE WORK

As discussed in previous sections, significant advances have been made in understanding the physics of flow-induced alignment of block copolymers. A unified three-dimensional mapping has integrated virtually all results on lamellar diblock copolymer melts published so far, and this mapping has been successfully applied to two-nanophase-separated ABC triblock copolymer melts as well. In addition to these three dimensions (temperature, frequency

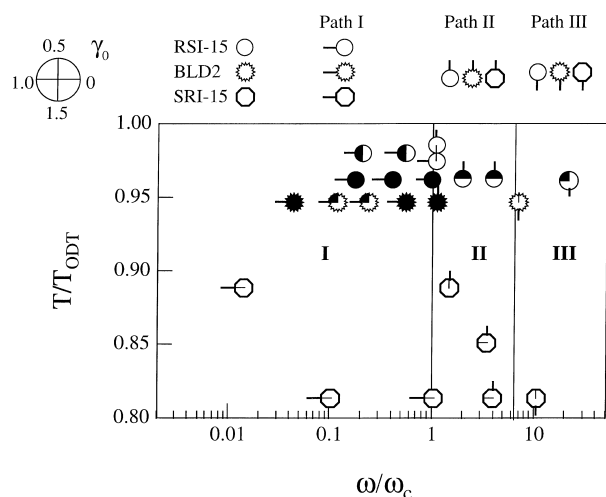


Figure 15 Flow-alignment behaviours of two-nanophase-separated lamellar ABC triblocks. BLD2 is a blend of two samples (RSI-20:RSI-15 = 1:4)

and strain amplitude), time has been explored as a fourth dimension.

Dimensionless frequencies describing a cascade of relaxations of polymer chains, nanophases and microdomains are the major parameters determining the flow-alignment behaviour of a given material. Characteristic frequencies ω_c' and ω_d appear to be the key players in this dimension. A robust, reproducible and precise method has been developed to measure ω_c' , but developing a method to determine ω_d remains a challenge.

Parameters related to other dimensions require further investigation to understand their effects on alignment behaviour. Clearly, a single dimensionless time is not sufficient to describe the kinetics along a given alignment trajectory, since strain amplitude affects the time scale differently in the fast and slow processes. Images of the microstructural changes in each process give insight into the reasons they behave differently; however, an explanation for their individual kinetics is still lacking. Similarly, the role of many other thermodynamic and dynamic parameters, such as the strength of segregation, chain mobility, viscoelastic contrast and entanglement, are not yet clear. The differences in alignment behavior of PEP-PEE-type and PS-PI-type diblock copolymers suggest that entanglement and/or viscoelastic contrast have interesting effects.

Further experimental work that addresses issues such as the effects of entanglement and viscoelastic contrast in determining flow alignment behaviour would involve the careful selection of experimental methods and the design and preparation of ideal model systems. The integrated approach including *in-situ* and *ex-situ* characterization provides an appropriate experimental means. The model systems should be designed in such a way that the gap in the degree of entanglement and viscoelastic contrast between PEP-PEE-type and PS-PI-type BCPs is filled.

The mechanisms proposed over the past two decades have been re-evaluated recently^{2,46,49,50,63}. Selective melting appears not to be widely important^{2,49,50,63}, while selective creation is strongly indicated when the initial condition is an unaligned state obtained by quiescent ordering^{2,63}. Grain rotation is supported by the rheo-optical signature of parallel alignment in Regime IV⁴⁶. Defect migration has been observed in many cases^{41,63} and the specific types of defects involved in different stages of

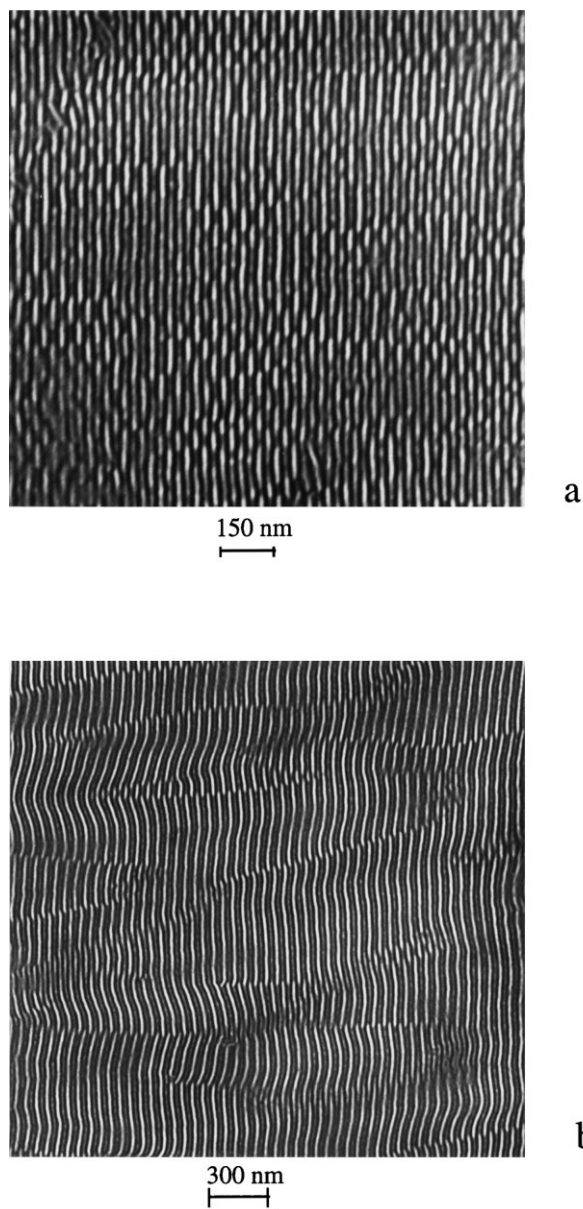


Figure 16 'Correlated perforations' in three-nanophase-separated lamellae of SIR-35. (a) A high defect density is observed in samples quenched from the two-nanophase state. (b) Coarsening occurs during annealing in the three nanophase state

alignment have been imaged for Regimes I, II and III⁶³. Many questions remain, such as the detailed mechanism(s) of flipping.

Experimental progress in understanding flow-induced alignment presents new opportunities in modelling and simulation, which in turn could yield valuable insights to guide the unified design of materials and processing conditions to exploit alignment phenomena. Observation of microstructural evolution at well-defined stages in each alignment trajectory provides a new perspective on the way theoretical and simulation work could be approached. Instead of focusing on the final aligned states^{34,35,37,39,42,44,47,48}, recent advances^{2,46,49–51,63} suggest that we should treat flow-induced alignment as a dynamic process³⁶. For each alignment trajectory, it may be possible to break the overall alignment process into parts that are tractable by analysis or simulation. For example, the conversion of poorly organized material into lamellae

might be treated as an individual part. This reorganization process would proceed differently at very high frequencies, where chain dynamics play an important role, from at low frequencies, where nanostructural dynamics dominate. Specific types of defect migration might be investigated theoretically as well. For example, the elimination of partial focal conic defects by oscillatory shear might be modelled to clarify the early fast process. The evolution of chevron patterns of defects under the influence of very high frequency ($\omega \gg \omega_c'$) oscillatory shear might be modelled, to gain insight into the slow process of the type-III trajectories to parallel alignment. Theoretical understanding of these individual processes will bring us closer to the goal of describing the whole alignment process.

As more elaborate nanostructures can be formed by ABC triblock copolymers and other types of BCPs with complex architectures, flow-induced alignment of these hierarchically organized nanostructures will deserve increasing attention. Many new questions regarding flow-induced alignment behaviours will be raised. For example, when cylinders are present at the interfaces between the lamellae in ABC triblock copolymers, does it alter the alignment behaviour of the lamellar superstructure? Are there parallel and perpendicular regimes for the layers? Do the cylinders orient along the flow direction? Chiral nanostructures could be produced by applying shear flow of a helix-on-cylinder morphology to discriminate between right- and left-handed helices. In the case of BCPs that have one side-group liquid crystalline polymer (SGLCP) block, one may deal with both the alignment of BCP layers and the director orientation in the SGLCP nanophase. Understanding the flow-induced alignment behaviours of these novel nanostructures would pave the way to developing new functional self-assembled materials.

REFERENCES

- Olson, G. B., *Science*, 1997, **277**, 1237; Attard, G. S. *et al.*, *Science*, 1997, **277**, 838.
- Chen, Z.-R., Kornfield, J. A., Smith, S. D., Grothaus, J. T. and Satkowski, M. M., *Science*, 1997, **277**, 1248.
- Muthukumar, M., Ober, C. K. and Thomas, E. L., *Science*, 1997, **277**, 1225.
- Decher, G., *Science*, 1997, **277**, 1232.
- Kumar, K. N. P. *et al.*, *Nature*, 1997, **358**, 48; Tolbert, S. H., Firouzi, A., Stucky, G. D. and Chmelka, B. F., *Science*, 1997, **278**, 264; Aksay, I. A., *Science*, 1996, **273**, 892.
- Tirrell, D. A., *Nature*, 1997, **390**, 336; Yu, S. J. M. *et al.*, *Nature*, 1997, **389**, 167.
- Stupp, S. I. and Braun, P. V., *Science*, 1997, **277**, 1242.
- Templin, M. *et al.*, *Science*, 1997, **278**, 1795.
- Wu, Z. and Grubbs, R. H., *Macromolecules*, 1994, **27**, 6700.
- Deming, T. J., *Nature*, 1997, **390**, 386.
- Aggeli, A. *et al.*, *Nature*, 1997, **386**, 259; Coyne, K. J., Qin, X. X. and Waite, J. H., *Science*, 1997, **277**, 1830.
- Mukamel, S., Tretiak, S., Wagersreiter, T. and Chernyak, V., *Science* 1997, **277**, 781; Weissman, J. M., Sunkara, H. B., Tse, A. S. and Asher, S. A., *Science*, 1996, **274**, 959.
- Park, M., Harrison, C., Chaikin, P. M., Register, R. A. and Adamson, D. H., *Science*, 1997, **276**, 1401; Chou, S. Y., Krauss, P. R. and Renstrom, P. J., *Science*, 1997, **272**, 85.
- Auschra, C. and Stadler, R., *Macromolecules*, 1993, **26**, 2171; Krappe, U., Stadler, R. and Voigt-Martin, I., *Macromolecules*, 1995, **28**, 4558; 1995, **28**, 7583.
- Mogi, Y. *et al.*, *Macromolecules*, 1994, **27**, 6755.
- Wei, Z. and Wang, Z.-G., *Macromolecules*, 1995, **28**, 7215.
- Tselikas, Y. *et al.*, *Macromolecules*, 1995, **29**, 2456.
- Pochan, D. J. *et al.*, *Macromolecules*, 1996, **29**, 5091.
- Ashraf, A. and Smith, S. D., submitted.
- Bates, F. S. and Fredrickson, G. H., *Annu. Rev. Phys. Chem.*, 1990, **41**, 525; Bates, F. S., *Science*, 1991, **251**, 898.

21. Bates, F. S. and Fredrickson, G. H., *Annual Rev. Mater. Sci.*, 1996, **26**, 501.
22. Colby, R. H., *Curr. Opin. Coll. Int. Sci.*, 1996, **1**, 454.
23. Morkved, T. L., Lu, M., Urbas, A. M., Ehrichs, E. E., Jaeger, H. M., Mansky, P. and Russell, T. P., *Science*, 1996, **273**, 931.
24. Keller, A., Pedemonte, E. and Willmouth, F. M., *Colloid Polym. Sci.*, 1970, **238**, 25.; Folkes, M. J. Keller, A. and Scalisi, F. P., *Colloid Polym. Sci.*, 1973, **251**, 1.
25. Hadziioannou, G., Mathis, A. and Skoulios, A., *Colloid Polym. Sci.*, 1979, **257**, 136; 1979, **257**, 15; Hadziioannou, G., Mathis, A. and Skoulios, A., *Macromolecules*, 1982, **15**, 258.
26. Morrison, F. A. and Winter, H. H., *Macromolecules*, 1989, **22**, 3533.; Morrison, F. A., Winter, H. H., Gronski, W. and Barnes, J. D., *Macromolecules*, 1990, **23**, 4200.
27. Chen, J. T., Thomas, E. L., Ober, C. K. and Mao, G. P., *Science*, 1996, **273**, 343.
28. Brehmer, M., Mao, G., Ober, C. K. and Zentel, R., *Macromolecular Symposia*, 1997, **117**, 175.
29. Quiram, J. D., Register, R. A., Marchand, G. R., submitted; Hamley, I. W., Patrick, J., Fairclough, A., Ryan A. J., Bates, F. S. and Towns-Andrews, E., *Polymer*, 1996, **37**, 4425; Kofinas, P. and Cohen, R. E., *Macromolecules*, 1995, **28**, 336; Shih, H. Y., Kuo, W. F., Pearce, E. M. and Kwe, T. K., *Polym. Adv. T.*, 1995, **6**, 417; Ryan, A. J., Hamley, I. W., Bras, W. and Bates, F. S., *Macromolecules*, 1995, **28**, 3860; Rangarajan, P., Register, R. A., Fetters, L. J., Bras, W., Naylor, S. and Ryan, A. J., *Macromolecules*, 1995, **28**, 4932; Nojima, S., Kato, K., Yamamoto, S. and Ashida, T., *Macromolecules*, 1992, **25**, 2237; Cohen, R. E., Cheng, P. L., Douzinas, K., Kofinas, P. and Berney, C. V., *Macromolecules*, 1990, **23**, 324; Khandpur, A. K., Macosko, C. W. and Bates, F. S., *J. Polym. Sci., B: Polym. Phys.*, 1995, **33**, 247; Sakurai, K., MacKnight, W. J., Lohse, D. J., Schultz, D. N. and Sissano, J. A., *Macromolecules*, 1993, **26**, 3236; Pepe, T., Schultz, M. F., Zhao, J., Tirrell, M. and Bates, F. S. *Macromolecules*, 1995, **28**, 3008; Schnablegger, H., Rein, D. H., Rempp, P. and Cohen, R. E., *J. Polym. Eng.*, 1995, **16**, 1; Robitaille, C. and Prud'homme, J., *Macromolecules*, 1983, **16**, 665; Seguela, R. and Prud'homme, J., *J. Polym.*, 1989, **30**, 1446.
30. Hillmyer, M. A., Lipic, P. M., Hajduk, D. A., Almdal, K. and Bates, F. S., *J. Am. Chem. Soc.*, 1997, **119**, 2747.
31. Zheng, W. Y. and Hammond, P. T., *Macromol. Rapid*, 1997, **17**, 11.
32. Antonietti, M. and Forster, S., in preparation.
33. Bruinsma, R. and Rabin, Y., *Phys. Rev. A*, 1992, **45**, 994.
34. Cates, M. E. and Milner, S. T., *Phys. Rev. Lett.*, 1989, **62**, 1856; Goulian, M. and Milner, S. T., *Phys. Rev. Lett.*, 1995, **74**, 1775.
35. Fredrickson, G. H., *J. Rheol.*, 1994, **38**, 1045.
36. Kodama, H. and Doi, M., *Macromolecules*, 1996, **29**, 2652.
37. Amundson, K., Helfand, E., Quan, X., Hudson, S. D. and Smith, S. D., *Macromolecules*, 1994, **27**, 6559; Mansky, P. and Russell, T. P. *Science*, 1996, **273**, 931; Amundson, K., Helfand, E., Davis, D. D., Quan, X., Patel, S. S. and Smith, S. D., *Macromolecules*, 1991, **24**, 6546.; Amundson, K., Helfand, E., Quan, X. and Smith, S. D., *Macromolecules*, 1993, **26**, 2698; Amundson, K. and Helfand, E., *Macromolecules*, 1993, **26**, 1324.
38. Shiota, A. and Ober, C. K., *Macromolecules*, 1997, **30**, 4274.
39. Koppi, K., Tirrel, M., Bates, F. S., Almdal, K. and Colby, R. H., *J. Phys. II*, 1992, **2**, 1941.
40. Koppi, K., Tirrel, M. and Bates, F. S., *Phys. Rev. Lett.*, 1993, **70**, 1449.
41. Winey, K. I., Patel, S. S., Larson, R. G. and Watanabe, H., *Macromolecules*, 1993, **26**, 2542.
42. Winey, K. I., Patel, S. S., Larson, R. G. and Watanabe, H., *Macromolecules*, 1993, **26**, 4373.
43. Larson, R. G., Winey, K. I., Patel, S. S. and Watanabe, H., *Rheol. Acta*, 1993, **32**, 245.
44. Riise, B. L., Fredrickson, G. H., Larson, R. G. and Pearson, D. S., *Macromolecules*, 1995, **28**, 7653.
45. Okamoto, S., Saijo, K. and Hashimoto, T., *Macromolecules*, 1994, **27**, 5547.
46. Kannan, R. M. and Kornfield, J. A., *Macromolecules*, 1994, **27**, 1177.
47. Patel, S. S., Larson, R. G., Winey, K. I. and Watanabe, H., *Macromolecules*, 1995, **28**, 4313.
48. Zhang, Y., Wiesner, U. and Spiess, H. W., *Macromolecules*, 1995, **28**, 778.
49. Gupta, V. K., Krishnamoorti, R., Kornfield, J. A. and Smith, S. D., *Macromolecules*, 1995, **28**, 4464.
50. Gupta, V. K., Krishnamoorti, R., Kornfield, J. A. and Smith, S. D., *Macromolecules*, 1996, **29**, 1359.
51. Gupta, V. K., Krishnamoorti, R., Chen, Z.-R., Kornfield, J. A., Smith, S. D., Satkowski, M. M. and Grothaus, J. T., *Macromolecules*, 1996, **29**, 875.
52. Pinheiro, B. S., Hajduk, D. A., Gruner, S. M. and Winey, K. I., *Macromolecules*, 1996, **29**, 1482.
53. Polis, D. L. and Winey, K. I., *Macromolecules*, 1996, **29**, 8180.
54. Hudson, S. D., Amundson, K. R., Jeon, H. G. and Smith, S. D., *Mat. Res. Soc. Bulletin*, 1995, **20**, 42.
55. Zhang, Y. M. and Wiesner, U., *J. Chem. Phys.*, 1995, **103**, 4784.
56. Zhang, Y., Wiesner, U., Yang, Y., Pakula, T. and Spiess, H. W., *Macromolecules*, 1996, **29**, 5427.
57. Zhang, Y. and Wiesner, U., *J. Chem. Phys.*, 1997, **106**, 2961.
58. Maring, D. and Wiesner, U., *Macromolecules*, 1997, **30**, 660.
59. Morrison, F. A., Mays, J. W., Muthukumar, M., Nakatani, A. I. and Han, C. C., *Macromolecules*, 1993, **26**, 5271.
60. Nakatani, A. I., Morrison, F. A., Douglas, J. F., Mays, J. W., Jackson, C. L., Muthukumar, M. and Han, C. C., *J. Chem. Phys.*, 1996, **104**, 1589.
61. Balsara, N., Hammouda, B., Kesani, P. K., Jonnalagadda, S. V. and Straty, G. C., *Macromolecules*, 1994, **27**, 2566; Balsara, N. P. and Hammouda, B., *Phys. Rev. Lett.*, 1994, **72**, 360; Balsara, N. P. and Dai, H. J., *J. Chem. Phys.*, 1996 **105**, 2942.
62. Wang, H., Kesani, P. K., Balsara, N. P. and Hammouda, B., *Macromolecules*, 1997, **30**, 982.
63. Chen, Z.-R., Issaian, A., Kornfield, J. A., Smith, S. D., Grothaus, J. T. and Satkowski, M. M., *Macromolecules*, 1997, **30**, 7096.
64. Lee, H. H., Register, R. A., Hajduk, D. A. and Gruner, S. M., *Polymer Engineering and Science*, 1996, **36**(10), 1414.
65. Albalak, R. J. and Thomas, E. L., *J. Polym. Sci.: Polym. Phys.*, 1993, **31**, 3766.
66. Rosedale, J. H. and Bates, F. S., *Macromolecules*, 1990, **23**, 2329.
67. Sakurai, K., MacKnight, W. J., Lohse, D. J., Schulz, D. N., Sissano, J. A., Wedler, W. and Winter, H. H., *Polymer*, 1996, **37**, 5159.
68. Kawasaki, K. and Onuki, A., *Physical Review A*, 1990, **42**, 3664.
69. Rubinstein, M. and Obukhov, S. P., *Macromolecules*, 1993, **26**, 1740.
70. Chung, C. I. and Gale, J. C., *J. Polym. Sci. Polym. Phys. Ed.*, 1976, **14**, 1149; Chung, C. I. and Lin, M. I., *J. Polym. Sci. Polym. Phys. Ed.*, 1978, **16**, 545; Gouinlock E. V. and Porter, R. S., *Polym. Eng. Sci.*, 1977, **17**, 535.
71. Tepe, T., Hajduk, D. A., Hillmyer, M. A., Wiemann, P. A., Tirell, M., Bates, F. S., Almdal, K. and Mortensen, K., *J. Rheology*, 1997, **41**, 1147.
72. Chen, Z.-R., Ph.D. thesis, Caltech, 1997.
73. Scott, D. B., Waddon, A. J., Lin, Y.-G., Karasz, F. E. and Winter, H. H., *Macromolecules*, 1992, **25**, 4175.
74. Giddo, S. P. and Thomas, E. L., *Macromolecules*, 1997, **30**, 3739; 1994, **27**, 849; 1993, **26**, 4506.
75. Laurer, J. H., Hajduk, D. A., Fung, J. C., Sedat, J. W. and Smith, S. D., *Macromolecules*, 1997, **30**, 3938.
76. Allan, P., Arridge, R. G. C., Ehtaiatkar, F. and Folkes, M. J., *J. Phys. D: App. Phys.*, 1991, **24**, 1381.
77. Lodge, T. P. and Fredrickson, G. H., *Macromolecules*, 1992, **25**, 5643.
78. Hongladarom, K., Burghardt, W. R., Baek, S. G., Cementwala, S. and Magda, J. J., *Macromolecules*, 1993, **26**, 772; Hongladarom, K., Ugaz, V. M., Cinader, D. K., Burghardt, W. R. and Quintana, J. P., *Macromolecules*, 1996, **29**, 5346.
79. Kalogriantis, S. G. and Van Egmond, J. W., *J. Rheol.*, 1997, **41**, 343.
80. Balsara, N. P., Perahia, D., Safinya, C. R., Tirrell, M. and Lodge, T. P., *Macromolecules*, 1992, **25**, 3896; Garetz, B. A., Newstein, M. C., Dai, H. J., Jonnalagadda, S. V. and Balsara, N. P., *Macromolecules*, 1993, **26**, 3151; Balsara, N. P., Garetz, B. A. and Dai, H. J., *Macromolecules*, 1993, **26**, 6072.
81. Garetz, B. A., Newstein, M. C., Dai, H. J., Jonnalagadda, S. V. and Balsara, N. P., *Macromolecules*, 1993, **26**, 3152; Balsara, N. P., Garetz, B. A. and Dai, H. J., *Macromolecules*, 1992, **25**, 6072; Balsara, N. P., Perahia, D., Safinya, C. R., Tirrell, M. and Lodge, T. P., *Macromolecules*, 1992, **25**, 3896.
82. Tcherkasskaya, O., Spiro, J. G., Ni, S. R. and Winnik, M. A., *J. Phys. Chem.*, 1996, **100**, 7114; Ni, S. R., Zhang, P., Wang, Y. C. and Winnik, M. A., *Macromolecules*, 1994, **27**, 5742.
83. Hashimoto, T., Shibayama, M. and Kawai, H., *Macromolecules*, 1980, **13**, 1237; Mayes, A. M. and Olvera de la Cruz, M., *J. Chem. Phys.*, 1991, **95**, 4670.
84. Watanabe, H., *Macromolecules*, 1995, **28**, 5006.
85. Milner, S. T. and Witten, T. A., *Macromolecules*, 1992, **25**, 5495; Zhulina, E. B. and Halperin, A., *Macromolecules*, 1992, **25**, 5730; Masten, M. W. and Schick, M., *Macromolecules*, 1994, **27**, 187; Matsushita, Y., Nomura, M., Noda, I. and Imai, M., *Physica B*, 1995, **213**, 697.

86. Werner, A. and Fredrickson, G. H., *J. Polym. Sci.: Polym. Phys. Ed.*, 1997, **35**(5), 849.
87. Wang, Z.-G. and Chang, C., unpublished results.
88. Matsushita, Y., Nomura, M., Watanabe, J., Mogi, Y. and Noda, I., *Macromolecules*, 1995, **28**, 6007; Matsushita, Y., Tamura, M. and Noda, I., *Macromolecules*, 1994, **27**, 3680; Mogi, Y., Mori, K., Matsushita, Y. and Noda, I., *Macromolecules*, 1992, **25**, 5412; Mogi, Y., Kotsuji, H., Kaneko, Y. Mori, K., Matsushita, Y. and Noda, I., *Macromolecules*, 1992, **25**, 5408. Mogi, Y., Mori, K., Kotsuji, H., Matsushita, Y. and Noda, I., *Macromolecules*, 1993, **26**, 5169.
89. Gido, S. P., Schwark, D. W., Thomas, E. L. and Goncalves, M. D., *Macromolecules*, 1993, **26**, 2636.
90. Dormidontova, E. E. and Khokhlov, A. R., *Macromolecules*, 1997, **30**, 1980.
91. Breiner, U., Krape, U., Abetz, V. and Stadler, R., *Journal of Macromolecular Chemistry and Physics*, 1997, **198**(4), 1051; Bechmann, J., Auschra, C. and Stadler, R., *Macromol. Rapid Commun.*, 1994, **15**, 67; Balsamo, V., Vongydenfeldt, F. and Stadler, R., *Journal of Macromolecular Chemistry and Physics*, 1996, **197**(10), 3317; Breiner, U., Krappe, U. and Stadler, R., *Macromol. Rapid Commun.*, 1996, **17**(8), 567.
92. Abetz, V., Stadler, R. and Leibler, L., *Polymer Bulletin*, 1996, **37**, 135 Neumann, C., Abetz, V. and Stadler, R., *Polymer Bulletin*, 1996, **36**, 43.
93. Abetz, V. and Stadler, R., *Macro. Symp.*, 1997, **113**, 19. Stadler, R., Auschra, C., Beckmann, J., Krappe, U. and Voigtmartin I., *Macromolecules*, 1995, **28**, 3080.
94. Kane, L. and Spontak, R. J., *Macromolecules*, 1994, **27**, 1267.